

Received March 18, 2020, accepted April 8, 2020, date of publication April 20, 2020, date of current version May 14, 2020.

Digital Object Identifier 10.1109/ACCESS.2020.2989003

Solar Collectors Modeling and Controller Design for Solar Thermal Power Plant

SURENDER KANNAIYAN¹, NEERAJ DHANRAJ BOKDE^{1,2},
AND ZONG WOO GEEM³, (Member, IEEE)

¹Department of Electronics and Communication, Visvesvaraya National Institute of Technology, Nagpur 440010, India

²Department of Engineering—Renewable Energy and Thermodynamics, Aarhus University, Aarhus 8000, Denmark

³Department of Energy IT, Gachon University, Seongnam 13120, South Korea

Corresponding author: Zong Woo Geem (geem@gachon.ac.kr)

This work was supported by the Energy Cloud Research and Development Program through the National Research Foundation of Korea (NRF) funded by the Ministry of Science, ICT under Grant 2019M3F2A1073164.


ABSTRACT Electric power generation techniques utilizing solar energy urge scientists to research and develop technologies using sustainable resources on a large scale with qualities close to the ideal resource. Solar collectors are crucial components of a Solar Thermal Power plant (STP) which are required to be within a certain feasible range in order to operate and provide solar thermal resources and intermittent inputs. The closed-loop controller design for solar collectors enhances the lifespan of STP. This paper presents first principle modeling of Parabolic Trough Collector (PTC) using therminol oil and Linear Fresnel Reflector (LFR) design using water as working fluid. Using step test method linear transfer function obtained at continuous and discrete domain nominal operating range. A continuous Proportional Integral (PI) controller is designed either with Static Feed Forward (SFF) control or with Predictive Function Control (PFC). Optimal performance of the controller is based on performance indicators obtained through various case studies.

INDEX TERMS Solar thermal power plant, proportional integral, parabolic trough collector, linear fresnel reflector, static feed forward, predictive function control.

I. INTRODUCTION

Industrial development from automation to electricity over time has always been fueled by energy sources. These sources of energy are primarily dominated by naturally occurring resources such as coal, oil, natural gas, etc. Considering the increasing demand of a better lifestyle and a more technologically advanced society, these naturally occurring resources are being exploited at an unprecedented rate [1].

The reckless use of energy resources has taken a toll on nature and has caused significant environmental damage. The climate has experienced changes due to the greenhouse and carbon cycle effects. Hotter days and longer dry periods are indicators of increasing temperatures; over the 21st century, the global temperature increased from 0.6 to 0.9 °C [2]. Chlorofluorocarbons (CFC) pose a threat to the ozone. The Global Warming Potential (GWP) is a relative measure of how much a particular gas contributes to global warming,

The associate editor coordinating the review of this manuscript and approving it for publication was Padmanabh Thakur .

having a baseline of one for the Carbon dioxide molecule [3]. The combustion of fossil fuels results in the production of the major greenhouse gas carbon dioxide (CO₂), which causes global warming and climate change [4]. The concentration of gas is measured in terms of particles per million (ppm). The critical value for this greenhouse gas is 350 ppm; if this value is exceeded, there may be unpredictable climate changes. Since 1998, the amount of this greenhouse gas has crossed the critical limit of 350 ppm. The amount of emission of this gas has gradually increased from the 1950's [5].

There are alternate ways to generate electricity with the use of renewable energy. This renewable energy is generated from natural processes that are continuously replenished over time. Electricity can be generated from solar, wind, hydroelectric, geothermal, and nuclear forms of energy [6].

Solar energy has been the predominant choice preferred over all others based on the following factor. The immensity of solar energy reaching the earth, along with its synchrony with the peak usage time of the day has made it one of the most promising sources of energy. The direct use of solar

radiation is our planet's chief resource. The mathematics behind this providing a supportive stance is as follows: 60% of the 1.8×10^{14} kW of solar energy received by earth reaches the surface, whereas the rest is reflected and absorbed by the atmosphere [7].

Solar power generation [8] can be obtained by two different methods, namely Photovoltaic and solar thermal.

- The Photovoltaic (PV) method uses semi-conductor technology [9] to directly convert sunlight into electricity. This technology generates power when solar radiation is present [10] and the battery stores it as electric energy [11], [12].
- In the solar thermal power conversion technique, solar collectors are used to concentrate sunlight to prepare high-temperature heat for the Rankine cycle. The Rankine cycle is used to drive the steam turbine with superheated vapor. The steam turbine's shaft is connected to a generator to produce electricity. This thermal plant has the added advantage of directly storing heat energy.

Solar thermal technology consists of four common components: a concentrator, receiver, heat transfer fluid, and power conversion. It is either classified as a single axis or two-axis tracking technology, or as a line or point technology. The category of single-axis tracking technology or the line focus technology mainly comprises of the parabolic trough and linear Fresnel reflector technologies. The category of the two-axis tracking technology or the point focus technology consists of the central receiver and parabolic dish technologies.

This hybrid solar plant design consisting of solar heat energy is transferred to oil in PTC, whereas water is used in LFR as the heat transfer fluid. A two-phase flow occurs in LFR; whereas a single-phase flow occurs in PTC.

(i) Parabolic Trough Collector (PTC) Technology [6]:

- Consists of parabolic reflectors as concentrators, rays to be focused on the focal line.
- Provided with a single-axis tracking mechanism with East to West, or North to South track.
- Conventional steam turbines are driven with high-temperature heating.
- Advantages: Reliable, commercially proven, and mature. Modularity, scalability, and storage pave the way for significant heat production. Cost-effective and uses less land compared to the central receiver and parabolic dish technologies.
- Disadvantages: High-cost investment, limitation of operating temperature, a stable structure required.

(ii) Linear Fresnel Reflector (LFR) Technology [6]:

- It flattens the parabolic trough reflector into a set of rows capable of tracking the sun about one axis, and directs the solar power on to a fixated downward-facing receiver parallel to the reflectors' rotational axis.
- Advantages: Reduced support structure, ball joints eliminated, land usage and cost reductions, easier to clean.
- Disadvantages: Accommodation for thermal storage capacity is challenging, low thermal performance, and complex tracking mechanism.

A safe and economical operation is the most important factor for the STP and its power plant components. In case of emergency and fault occurrence, a sequence of operation is necessary. Interlock operation in a power plant helps to provide the necessary output from the plant components or helps to prevent the trip of plant components.

In this study, first principle modeling is considered for PTC and LFR, by which proper selection of manipulated and control variables are fitted for both system transfer functions. Certain operating points are fixed in both systems; a step test is performed, and the transfer function is fitted.

The transfer function is obtained based on the tolerance error between the fitted transfer function and the output of system control variable. The obtained transfer function is a continuous first-order model; it is converted to a discrete first-order system using zero-order hold. Based on the fitted transfer function, IMC tuning is opted for the continuous PI controller design; and based on the energy balance equation, the static feed-forward controller is also designed and combined for control. The PFC controller is designed based on the model identified and can inherently tolerate the uncertainty of the model parameters. These two types of controllers are implemented for both, PTC and LFR, and are analyzed individually. The optimal controller is chosen based on performance indicators and manipulated variable variation with physical reliability.

This study is organized as follows: section 2 provides a brief literature review of the control problems related to solar collectors; section 3 presents modeling of solar collectors using the first principle approach. Sections 4, 5, and 6 present design of the control system, controller (PID and PFC) design, and controller performance based on case study simulations of solar collectors; respectively. Section 7 presents the concluding remarks. Table 1 shows the list of abbreviations used throughout paper.

II. RELATED WORK

In this section, several literature reviews of studies relative to the closed-loop controller design of the solar collector are briefly discussed.

A. PTC

Conventional controllers (PID, FF, Cascade) are implemented at operating condition regions for better performance [13]. PID is a suitable controller for PTC with proper system identification; it is tuned where the controller performance is slow and does not react to a rapid disturbance due to the high time constant. Feedback PID and Feed Forward (FF) controllers can perform better with a measurable disturbance [14], [15]. Several advance control techniques are also implemented for PTC, which are briefly presented in the article [16].

Johansen *et al.* [17] presented three operating points for a PTC with linear models designed with a gain scheduling controller, suggesting additional operating points should be investigated for better performance.

TABLE 1. List of abbreviations.

ARAX	Autoregressive Exogenous
ARMAX	Autoregressive Moving Average with-Exogenous Inputs
C-PFC	Constant input with PFC control
C-PI	Constant input with PI and static feed-forward control
C-open	Constant Input open loop operation
CARIMA	Controlled Auto-Regressive Integrated-Moving Average
CFC	Chlorofluorocarbons
CO ₂	Carbon-dioxide
CV	Control Variable
DSG	Direct Steam Generation
FF	Feed-Forward
FO	First order
GPC	Generalized Predictive Controller
GWP	Global Warming Potential
HTF	Heat Transfer Fluid
IMC	Interanl Model Control
LFR	Linear Fresnel Reflector
MIMO	Multiple Input Multiple Output
MPC	Model Predictive Control
MV	Manipulated Variable
PDE	Partial Differential Equation
PFC	Predictive Function Control
PI	Proportional Integral
PID	Proportional Integral Derivative
ppm	particles per million
PTC	Parabolic Trough Collector
PV	Photo-Voltaic
SD	Steam Drum
SFF	Static Feed Forward
SISO	Single input and single output
STP	Solar Thermal Power plant
UKF	Unscented Kalman Filter
V-PFC	Varying input with PFC control
V-PI	Varying input with PI
V-open	Varying Input open loop operation
ZOH	Zero Order Hold

Camacho and Berenguel [18] proposed a gain-scheduling Generalized Predictive Controller (GPC) and a nonlinear prediction model to compute the control moves for a linear incremental model of PTC.

Silva *et al.* [19] presented the implementation of varying sampling intervals for PTC manipulated variable use; an adaptive pole placement controller was implemented for PTC on the real plant. Dual-mode MPC implementation with the higher model indicated that this method is feasible and suited for a wide range of operating regions [20].

Gallego and Camacho [13] designed a Model Predictive Control (MPC) to control the oil outlet temperature with the Unscented Kalman Filter (UKF); an estimation technique is

implemented for the approximation of solar radiation and absorber pipe temperature.

When the oil flow rate going into the PTC has excited with a sinusoidal variation, the heat gain of the outlet oil temperature at a specific point in the PTC length of the pipe is zero; this process is known as anti-resonance modes [18]. The resonant modes in PTC are important parameters needed to indicate when the flow rate of the oil is low. Higher-order dynamics are required to capture this effect. This factor is less dominant when the flow rate is high.

A linear model of PTC around the operating point was discussed in literature [14]. First-order step type model identification is obtained for PTC and subsequently, the conversion to discrete-time and PI controller design is also implemented [21].

This has been chosen as the control in many studies, and variables were manipulated with several controller techniques such as feedback linearization, Fuzzy, GPC, gain scheduling, etc. [14], [16]. It is implemented with PFC in the proposed system.

B. LFR

Domínguez *et al.* [22] stated that two types of control actions have been presented (1) feedwater flow rate control (2) feedwater enthalpy control. For feedwater flow rate control, the mass flow rate of water is created as a manipulated control variable to maintain the mass flow rate of steam. For feedwater enthalpy control, the input enthalpy of water is manipulated to control the generated steam flow rate in LFR. A high level of steam generation is achieved through feedwater enthalpy control and is proven to have poor process behavior compared to feed water flow rate control.

Aurousseau *et al.* [23] performed a brief review of control methods implemented in direct steam generation. In this article, controller implementation of direct steam generation on one trough, re-circulation, and injection mode is implemented. The system identification of a linear model of LFR is obtained through a step test, and is PI tuned for DSG type re-circulation mode.

Valenzuela *et al.* [24] indicated outlet steam temperature and pressure out of LFR is controlled by the manipulated variable of the inward water flow rate. The controller system is developed with system identification through a step test, and the PI controller is tuned to obtain the respective linear transfer function.

PTC has been used in direct steam generation by maintaining the steam flow rate out of LFR, which is controlled by the mass flow rate of water into the LFR. The level of water in SD is maintained at a constant. The PI controller was implemented for the re-circulation mode direct steam system, along with an additional level controller for the steam drum [25].

III. MODELING OF SOLAR COLLECTORS

Modeling the entire hybrid solar power plant is a critical task considering all the factors for real-time inputs

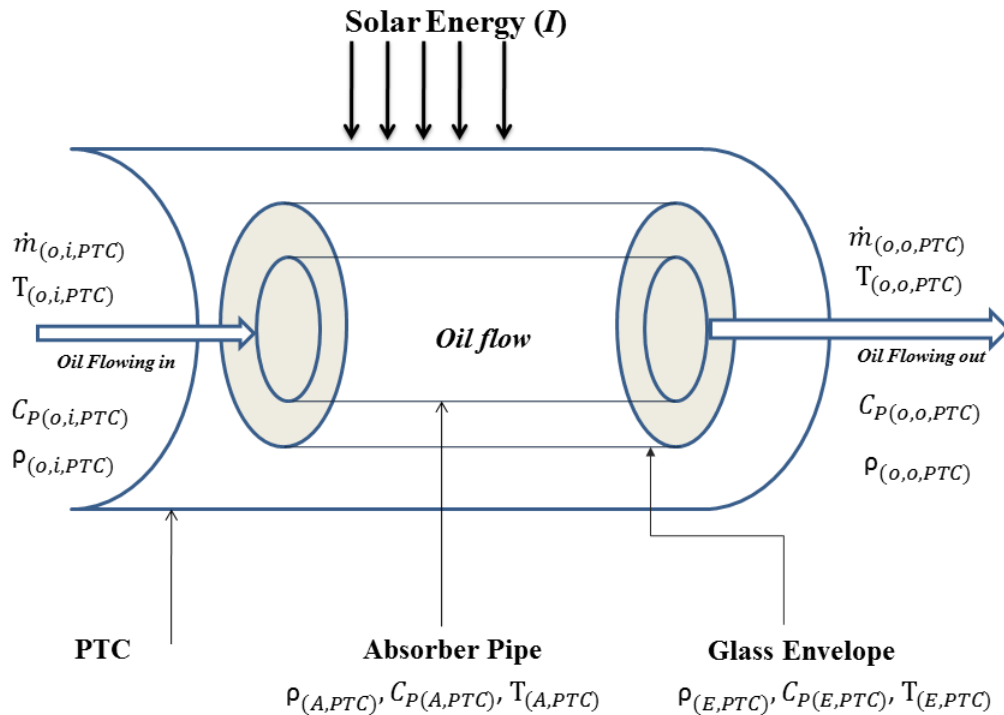


FIGURE 1. Schematic of PTC and receiver tube.

and effects. Various modeling approaches have been conducted and reported by several authors, with differences in relaxing certain factors in their modeling approach [26], [27]. If a sufficient modeling effort is constructed by appropriately considering major factors, the controller design for set-point operation and an effective power plant operation based on optimization requires less effort. Solar collectors, such as Parabolic Trough Collector (PTC) and Linear Fresnel Reflector (LFR,) play an important role in STP for the production of electricity through thermal energy. In this study, a hybrid solar thermal plant design and its parameters used for simulation are obtained from the literature Kannaiyan et al.. The operating solar collector within a certain range assists in achieving the production of electricity based on load conditions with minimal loss.

1) PARABOLIC TROUGH COLLECTOR (PTC)

The PTC consists of three components: therminol oil, absorber pipe (or receiver tube), and glass envelope, as shown in Figure 1. The therminol oil serves as a heat transfer fluid (HTF) and flows through the absorber pipe, whereas the glass envelope protects the absorber and reduces reflective losses by transmitting most of the incoming shortwave solar irradiation to the absorber pipe [29]. These components are represented as Spatio-temporal variations of the temperatures as $T_{(o,PTC)}(t, x)$, $T_{(A,PTC)}(t, x)$ and $T_{(E,PTC)}(t, x)$ for the therminol oil, absorber pipe, and glass envelope, respectively. These variations are governed by the following Partial Differential Equations (PDEs) obtained by the conservation of energy [29]:

The constant parameters and notations used in Equations (1a)-(1c), at the bottom of the next page, are described in Table 2.

The first and second terms on the right side of the Equation (1a) signify the net convective energy change in the fluid and the heat received due to convective heat transfer from the hot absorber pipe, respectively.

The energy balance for the glass envelope in Equation (1c) includes the radiative, as well as convective losses, to the atmosphere. To extract maximum energy from solar renewable energy instead of manipulating the oil flow rate through the PTC, it could be obtained by manipulating the optical efficiency of PTC. Investigation of optical efficiency gives scope in another domain. Liang et al. [30] used four different optical methods to evaluate the optical efficiency of PTC that relates through photon distribution. Zheng et al. [31] developed a new serpentine compound parabolic concentrator which is a combination of the compound parabolic concentrator and a flat-plate solar collector as solar collector module and stated that consists of thermal efficiency are higher, reduce heat loss for space heating at cold regions. Since this approach requires a support structure of PTC should need to investigate with a higher cost, so an alternative method of manipulating the oil flow rate through PTC has opted. The optical efficiency is assumed to be a constant parameter in the current study but it can be estimated online [32].

2) LINEAR FRESNEL REFLECTOR (LFR)

Linear Fresnel Reflector (LFR) consists of flat mirrors that focus sunlight on a receiver pipe similar to schematic of PTC.

TABLE 2. PTC: Notation and values of parameters.

Symbol	Description	Units	Values
$A_{(Aj,PTC)}, A_{(Ej,PTC)}$	($j = i$) Inner and ($j = o$) outer Cross-sectional area: absorber pipe and glass envelope respectively	m^2	$1.9e^{-3}, 2.8e^{-3}$
$C_{p(A,PTC)}, C_{p(E,PTC)}, C_{p(o,PTC)}$	Specific heat capacity: absorber pipe, glass envelope and HTF	J/kg/K	460 [29], 840 [29], function of temperature
$h_{(air,PTC)}, h_{(p,PTC)}$	Convective heat transfer coefficient Air-glass envelope, HTC of HTF	$W/(m^2\text{ }^\circ\text{C})$	25, Dittus Bolter equation [29]
I	Solar radiation incident on PTC collector surface	W/m^2	
$\dot{m}_{(o,i,PTC)}$	Mass flow rate of HTF flowing in	kg/s	3
$P_{(Aj,PTC)}$	($j = i$) Inner and ($j = o$) outer absorber pipe perimeter respectively	m	0.157, 0.188
$r_{(Aj,PTC)}$	($j = i$) Inner and ($j = o$) outer absorber pipe radius respectively	m	0.025, 0.03
t	Time variable	s	
$T_{(A,PTC)}, T_{(E,PTC)}, T_{(o,PTC)}$	Temperature: absorber pipe, glass envelope, and HTF	$^\circ\text{C}$	Variable
$T_{(air)}, T_{(sky)}$	Temperature: ambient, effective sky temperature	$^\circ\text{C}$	25, 40
W_{PTC}	Width of mirror aperture	m	5.75
$\xi_{(A,PTC)}, \xi_{(E,PTC)}$	Emissivity: absorber pipe, glass envelope	-	0.18, 0.9
$\eta_{(opt,PTC)}$	Total optical efficiency of PTC	-	0.4
$\rho_{(A,PTC)}, \rho_{(E,PTC)}, \rho_{(o,PTC)}$	Density: absorber pipe, glass envelope and HTF	kg/m^3	7850 [29], 2400 [29], function of temperature
σ	Stefan-Boltzmann constant	$W/(m^2K^4)$	$5.67e^{-8}$

This pipe carries water or a two-phase mixture to a steam drum called Direct Steam Generation (DSG) [22].

Parameters for the modeling of LFR are taken from the 1Mwe plant [28], there are a total of eight receiver tubes in the design as shown in equation 2. The dynamics of one receiver tube are modeled and it is assumed that the remaining receiver LFR behaves similarly.

$$\dot{m}_{(w,i,LFR)} = 8 * \dot{m}_{(w/8,i,LFR)} \tag{2}$$

LFR involves the flow of a two-phase water-steam mixture in the receiver pipe, whereas PTC involves the flow of heat transfer fluid in the liquid phase. For the water-steam mixture, in addition to mass and energy conservation, the modeling of momentum conservation is necessary for the coupling of mass continuity with pressure along the pipe. In this study, generation of the two-phase water-steam mixture model is obtained by adapting Chatoorgoon [33], which was originally developed to quantify the rate of steam generation

$$\frac{\partial T_{(o,PTC)}}{\partial t} (\rho_{(o,PTC)} C_{p(o,PTC)} A_{(Ai,PTC)}) = \dot{m}_{(o,i,PTC)} C_{p(o,PTC)} \frac{\partial T_{(o,PTC)}}{\partial x} + h_{(p,PTC)} P_{(Ai,PTC)} (T_{(A,PTC)} - T_{(o,PTC)}) \tag{1a}$$

$$\rho_{(A,PTC)} C_{p(A,PTC)} A_{(Ao,PTC)} \frac{\partial T_{(A,PTC)}}{\partial t} = h_{(p,PTC)} P_{(Ai,PTC)} (T_{(o,PTC)} - T_{(A,PTC)}) - \frac{\sigma}{\xi_{(A,PTC)} \frac{1-\xi_{(E,PTC)}}{\xi_{(E,PTC)}} \left(\frac{r_{(Ao,PTC)}}{r_{(Ei,PTC)}} \right)} P_{(Ao,PTC)} (T_{(A,PTC)}^4 - T_{(E,PTC)}^4) + I \eta_{(opt,PTC)} W_{PTC} \tag{1b}$$

$$\rho_{(E,PTC)} C_{p(E,PTC)} A_{(Eo,PTC)} \frac{\partial T_{(E,PTC)}}{\partial t} = \frac{\sigma}{\xi_{(A,PTC)} \frac{1-\xi_{(E,PTC)}}{\xi_{(E,PTC)}} \left(\frac{r_{(Ao,PTC)}}{r_{(Ei,PTC)}} \right)} P_{(Ai,PTC)} (T_{(A,PTC)}^4 - T_{(E,PTC)}^4) - \sigma \xi_{(E,PTC)} P_{(Eo,PTC)} (T_{(E,PTC)}^4 - T_{(sky)}^4) - h_{(air,PTC)} P_{(Eo,PTC)} (T_{(E,PTC)} - T_{(air)}) \tag{1c}$$

in a nuclear reactor. This model assumes a 1-d flow and computes the pressure drop and heat transfer coefficients using a homogeneous two-phase model. The water at the end of the LFR receiver pipe is either in a liquid phase, or is a two-phase mixture and enters the Steam Drum (SD), depending on the entering water condition and the prevalent solar radiation. The following equations describe the dynamic mass, energy, momentum, absorber pipe temperature, and glass pipe temperature.

$$\text{Mass: } \frac{\partial \rho}{\partial t} + \frac{\partial(\rho u)}{\partial x} = 0 \tag{3a}$$

$$\text{Momentum: } \frac{\partial(\rho u)}{\partial t} + \frac{\partial(\rho u^2)}{\partial x} + \frac{\partial P}{\partial x} + C_k \rho u^2 + \rho g = 0 \tag{3b}$$

$$\text{Energy: } \frac{\partial}{\partial t} \left[\rho \left(h + \frac{u^2}{2} \right) \right] + \frac{\partial}{\partial x} \left[\rho u \left(h + \frac{u^2}{2} \right) \right] + \rho u g = \frac{\partial P}{\partial t} + q_w \tag{3c}$$

$$\text{Equation of state: } \rho = f(P, h) \tag{3d}$$

The notations and the corresponding values of parameters for the LFR model presented in the above equations are tabulated in Table 3.

The mass continuity Equation (3a) is pressure linked through the Equation of state (Equation (3d)) which necessitates the simultaneous solution of Equations (3a)-(3d), along with the equations representing temperature variations in the absorber pipe and glass envelope (Equations (4a) as well as (4b)), at the bottom of the next page, to obtain the Spatio-temporal variation of density, enthalpy, pressure, and velocity of the fluid in the LFR tubes since the flow is compressible.

The energy conservation equations for the absorber pipe and the glass envelope are similar to PTC and are shown below:

The LFR model Equations (3a)-(4b) use various correlations for friction factors and heat transfer coefficients for single and two-phase flows in both, laminar and turbulent conditions. Furthermore, the rate of steam generation and water exiting the LFR are given as follows:

$$\dot{m}_{(st,o,LFR)} = (q|_{x=L}) \dot{m}_{(w,i,LFR)} \tag{5}$$

$$\dot{m}_{(w,o,LFR)} = \dot{m}_{(w,i,LFR)} (1 - (q|_{x=L})) \tag{6}$$

$$\text{where } q|_{x=L} = \frac{(h|_{x=L}) - (h_l|_{x=L})}{(h_v|_{x=L}) - (h_l|_{x=L})} \tag{7}$$

steam quality at the exit of the LFR tube with subscripts *l* and *v* representing saturated liquid and saturated vapor. The quality of steam inherently represents the mass flow rate of steam exiting the LFR ($\dot{m}_{(st,o,LFR)} = Q * \dot{m}_{(w,i,LFR)}$), whereas the mass flow rate of water flowing out of the LFR ($\dot{m}_{(w,o,LFR)} = (1 - Q) * \dot{m}_{(w,i,LFR)}$) which are all related to the output variable (quality of steam).

Detail modeling of LFR and conversion of the stiff differential equation to the difference equation, as well as the algorithm for implementation of LFR are explained in detail in appendix A.

IV. DESIGN OF CONTROL SYSTEM

In a real-time control system, the two major tasks are as follows: (1) Servo Problem - Setpoint tracking (2) Regulator Problem - Disturbance tracking. The performance of the control system should be robustly subjected to change in the dynamics of the process, measurement model, and actuators. For a few cases, the disturbance and measurement noises are not measurable; they have an impact on the output variable. The block diagram is shown in Figure 3, which represents a general block diagram of the control system; depending on several variables (input, disturbances, and output), it can be extended to Multi-input and Multi-output (MIMO).

Based on the above constraints, an appropriate loop shaping is required to design a proper achievable controller for real-time implementation.

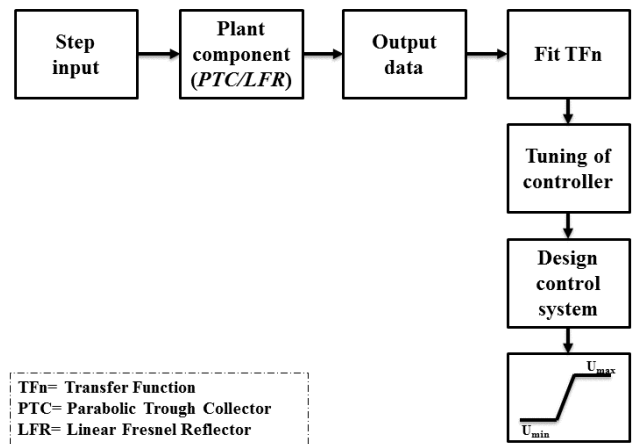


FIGURE 2. Algorithm for control system design.

The design of a proper control system requires four sequences of steps to be followed as shown in Figure 2 and described as follows:

- 1) Step test is performed for solar plant components (PTC, LFR) by applying a step input on its manipulated variable.
- 2) Following the application of the step input control variable (CV), the output data is collected.
- 3) Transfer function is fitted to match the behavior of PV data. Transfer function parameters were tuned to obtain less tolerance.
- 4) Controller tuning parameters are obtained based on the fitted transfer function and Internal Model Control (IMC) tuning rules as shown in Table 5.

A. SYSTEM IDENTIFICATION

In real-time modeling, a physical plant and its components with the first principle approach are complex; since most of the system is nonlinear, in order to obtain the linear model from its nonlinear nature it should be linearized at several operating points. In a single input and single-output (SISO) system, most of the tuning algorithms of controllers are based on empirical models. Therefore, it is necessary to obtain the

TABLE 3. LFR: Notation and values of parameters.

Symbol	Description	Units	Values
$T_{(w/st/2\phi,LFR)}$	Temperature of water/steam/ two phase mixture depending on operating condition	$^{\circ}\text{C}$	
ρ	Density of working fluid	kg/m^3	
h	Specific enthalpy of working fluid	J/kg	
u	Velocity flow velocity of working fluid	m/s	
P	Pressure	bar	
C_k	Friction constant		
q_w	Heat per unit volume of flow (refer A.3)	W/m^3	
$A_{(A,LFR)}, A_{(E,LFR)}$	Cross-sectional area: absorber pipe and glass envelope	m^2	$5e^{-4}, 7e^{-4}$
$C_{p(A,LFR)}$ and $C_{p(E,LFR)}$	Specific heat capacity: absorber pipe and glass envelope	J/kg/K	460 [29], 840 [29], Function of temperature
$h_{(air,LFR)}, h_{(p,LFR)}$	Convective heat transfer coefficient air-glass envelope, HTC of working fluid	$\text{W}/(\text{m}^2 \text{ } ^{\circ}\text{C})$	25, refer section S.2.1.2 [34]
I	Solar radiation incident on PTC collector surface	W/m^2	
$\dot{m}_{(w,i,LFR)}$	Mass flow rate of working fluid flowing in towards LFR	kg/s	0.3 (open loop)
$\dot{m}_{(w/8,i,LFR)}$	Mass flow rate of working fluid flowing in towards one receiver pipe	kg/s	0.3 (open loop)
$P_{(Aj,LFR)}$	($j = i$) Inner and ($j = o$)outer Absorber pipe perimeter respectively	m	0.084, 0.1963
$r_{(Aj,LFR)}$	($j=i$) Inner and ($j=o$) outer absorber pipe radius respectively	m	0.0135, 0.015
L	Length of LFR	m	480
$T_{(A,LFR)}, T_{(E,LFR)}$	Temperature: absorber pipe, and glass envelope	$^{\circ}\text{C}$	Variable
$T_{(air)}, T_{(sky)}$	Temperature: Ambient, effective sky temperature	$^{\circ}\text{C}$	25, 40
W_{LFR}	Width of mirror aperture	m	14
$\xi_{(A,LFR)}, \xi_{(E,LFR)}$	Emissivity: absorber pipe, glass envelope	–	0.18, 0.9
$\eta_{(opt,LFR)}$	Total optical efficiency of LFR	–	0.21
$\rho_{(A,LFR)}, \rho_{(E,LFR)}, \rho_{(o,LFR)}$	Density: absorber pipe, glass envelope and HTF	kg/m^3	7850 [29], 2400 [29], Function of temperature
σ	Stefan-Boltzmann constant	$\text{W}/(\text{m}^2 \text{K}^4)$	$5.67e^{-8}$
g	Gravitational acceleration	m/s^2	9.8

$$\rho_{(A,LFR)} C_{p(A,LFR)} A_{(A,LFR)} \frac{\partial T_{(A,LFR)}}{\partial t} = h_{(p,LFR)} P_{(Ai,LFR)} (T_{(w/st/2\phi,LFR)} - T_{(A,LFR)}) - \frac{\sigma}{\frac{1}{\xi_{(A,LFR)}} + \frac{1-\xi_{(E,LFR)}}{\xi_{(E,LFR)}} \left(\frac{r_{(Ao,LFR)}}{r_{(Ei,LFR)}} \right)} P_{(Ao,LFR)} (T_{(A,LFR)}^4 - T_{(E,LFR)}^4) + I \eta_{(opt,LFR)} W_{(LFR)} \quad (4a)$$

$$\rho_{(E,LFR)} C_{p(E,LFR)} A_{(E,LFR)} \frac{\partial T_{(E,LFR)}}{\partial t} = \frac{\sigma}{\frac{1}{\xi_{(A,LFR)}} + \frac{1-\xi_{(E,LFR)}}{\xi_{(E,LFR)}} \left(\frac{r_{(Ao,LFR)}}{r_{(Ei,LFR)}} \right)} P_{(Ai,LFR)} (T_{(A,LFR)}^4 - T_{(E,LFR)}^4) - \sigma \xi_{(E,LFR)} P_{(Eo,LFR)} (T_{(E,LFR)}^4 - T_{(sky)}^4) - h_{(air,LFR)} P_{(Eo,LFR)} (T_{(E,LFR)} - T_{(air)}) \quad (4b)$$

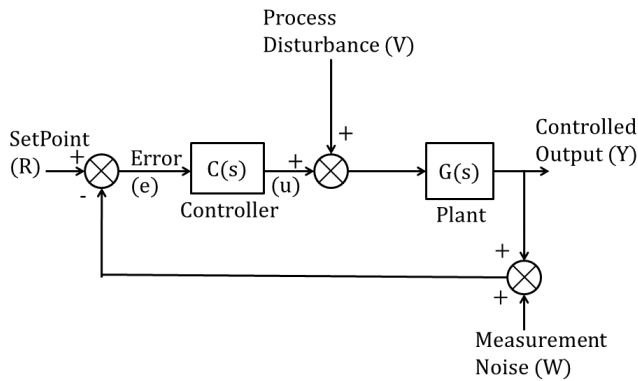


FIGURE 3. Block diagram of control system.

first or second-order model approximation. Approximation of the plant is essential for the control system, as shown in Figure 3, and less effort is required while designing and tuning the controller if the plant is identified properly. If the plant has significant uncertainty in its parameters, then the design and tuning of the controller becomes more complex. Several empirical model approximations such as the First-order (FO), and second-order approximations can be obtained in the discrete-time system, which is approximated by ARX, ARMAX, and CARIMA and are based on input and output data. Out of several approximations, the optimal one is based on the nature of the operating conditions and complexity.

Out of several approximation methods, the First Order (FO) model is opted for continuous and discrete models compared to other techniques based on simplicity in implementation.

1) SYSTEM IDENTIFICATION THROUGH FIRST ORDER MODEL

First Order (FO) based system identification consists of two parameters (process gain, the time constant) that need to be computed based on the process explained above; a relevant expression is shown in equation 8. Using the process reaction curve method, the FO model is obtained for the physical process. In this step test, process gain (K_p) is obtained based on the ratio of change in the magnitude of output, to change in the magnitude of input (manipulated variable). The time constant (τ) is obtained by predicting the time taken for the output variable to reach a 63% of change in the output variable to its steady-state value.

$$G(s) = \frac{K_p}{\tau s + 1} \tag{8}$$

Discrete Time first-order system (Z transform) In this approximation approach, the system approximation obtained from the continuous first-order model is converted to a first-order discrete-time model using Zero Order Hold (ZOH).

Parameters of the FO model (K_p, τ) are obtained based on the error value persisting between the fitted Transfer function

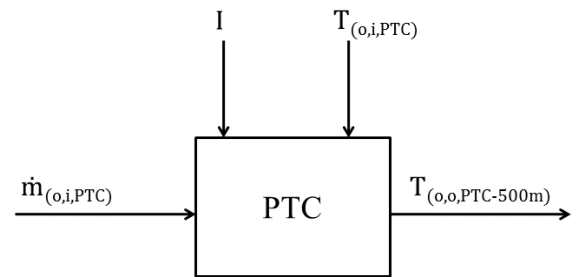
and the control variable output, as shown below:

$$Tol_{TF} = \int_0^t (P_{op} - FT_{if})dt \tag{9}$$

where P_{op} represents the control variable output (CV), FT_{if} represents the fitted transfer function profile output which is obtained from equation 8, and Tol_{TF} represents the tolerance value obtained as shown in equation 9 over the time period of computation.

2) PARABOLIC TROUGH COLLECTOR (PTC)

The first order linear transfer function of PTC is obtained by choosing the mass flow-rate of oil through PTC ($\dot{m}_{(o,i,PTC)}$) and the oil outlet temperature out of PTC ($T_{(o,o,PTC-500m)}$) as the manipulated and control variable, respectively, as shown in Figure 4.



$\dot{m}_{(o,i,PTC)}$ = mass flow rate of oil flow towards PTC

$T_{(o,i,PTC)}$ = Temperature of oil flow in towards PTC

$T_{(o,o,PTC-500m)}$ = Temperature of oil at PTC-500m

I= Solar Radiation

FIGURE 4. PTC control parameters.

While performing the step test of PTC, temperature of oil flow into PTC ($T_{(o,i,PTC)} = 326^{\circ}C$ to $200^{\circ}C$) and solar radiation ($I=600 \text{ w/m}^2$) is maintained constant and mass flow rate of oil flow into PTC with step change ($\dot{m}_{(o,i,PTC)} = 3$ to 4 kg/s) so the resultant temperature of oil out of PTC ($T_{(o,o,PTC-500m)}$) is collected as a control variable. While performing the step test, remaining certain input parameters kept constant for PTC, parameters are shown in Table 4.

A PTC first-order model is obtained for the continuous and discrete system by comparing the fitted transfer function of PTC with the oil energy balance equation (1a), as shown in Figure 5. Based on the tolerance value (Tol_{TF}) of 983 for a 1-hour operation of the step test, parameters for continuous and discrete-time system models are obtained as shown in Table 4.

Simulation of PTC under the open-loop and closed-loop operation performed with initial conditions $200^{\circ}C$, $201^{\circ}C$ and $40^{\circ}C$ for oil, absorber and glass pipe, respectively. The partial differential equation is converted to the ordinary differential equation using backward difference and grid

TABLE 4. Controller parameters.

Parameters System	PTC	LFR
Manipulated Variable (MV)	Oil flow rate in towards PTC ($\dot{m}_{(o,i,PTC)}$)	Water flow rate in towards LFR ($\dot{m}_{(w,i,LFR)}$)
Control Variable (CV)	Oil outlet Temperature ($T_{(o,o,PTC-500m)}$)	Steam quality exit out of LFR ($Q_{(st,o,LFR)}$)
Disturbance	Optical Efficiency $\eta_{(opt,PTC)}$, Oil inlet temperature ($T_{(o,i,PTC)}$), Solar radiation(I)	Optical Efficiency $\eta_{(opt,LFR)}$, Inlet water temperature to LFR ($T_{(w,i,LFR)}$), Solar radiation(I)
First order(FO) Approximation (S domain)	$\frac{-28}{350S+1}$	$\frac{-0.448}{500S+1}$
Discrete Model First Approximation Domain (Z)	$\frac{-0.079}{Z-0.9971}$	$\frac{-0.0014}{Z-0.9967}$

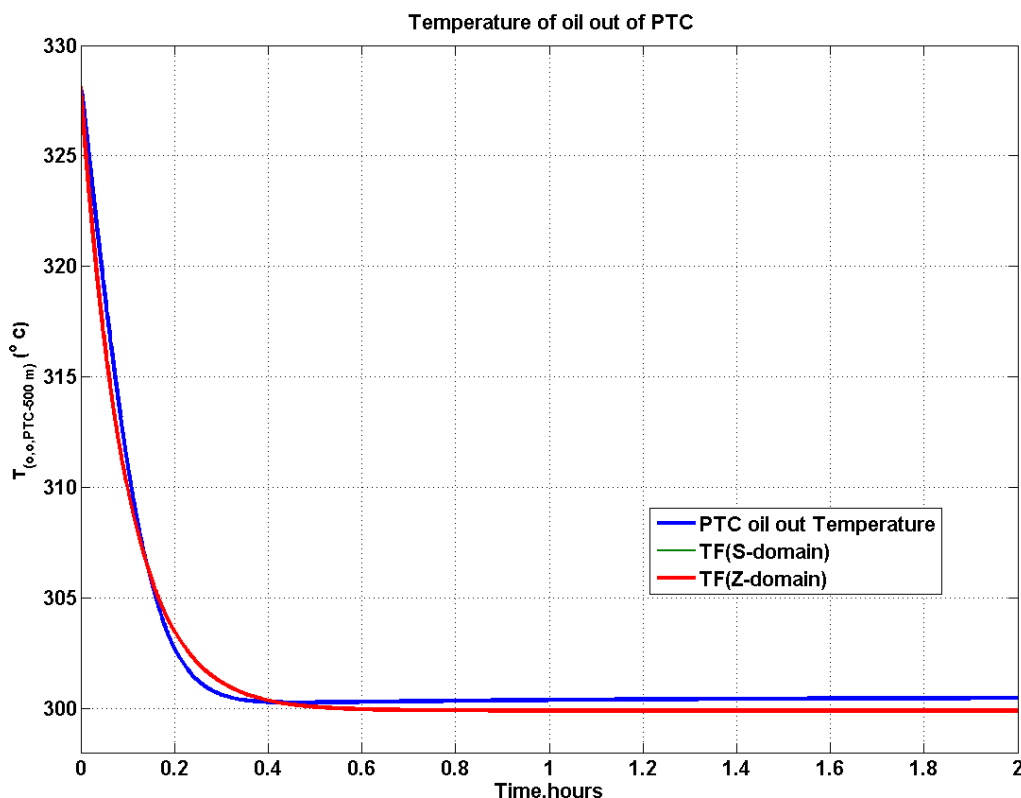


FIGURE 5. System Identification of PTC.

point computation is obtained with 15 for length 500 m of PTC [28]. Simulation of PTC and integration over-time period are simulated using the ode45 command in

MATLAB with a time interval of 1 second. During the disturbance condition disturbance of oil is simulated as shown in Figure 8.

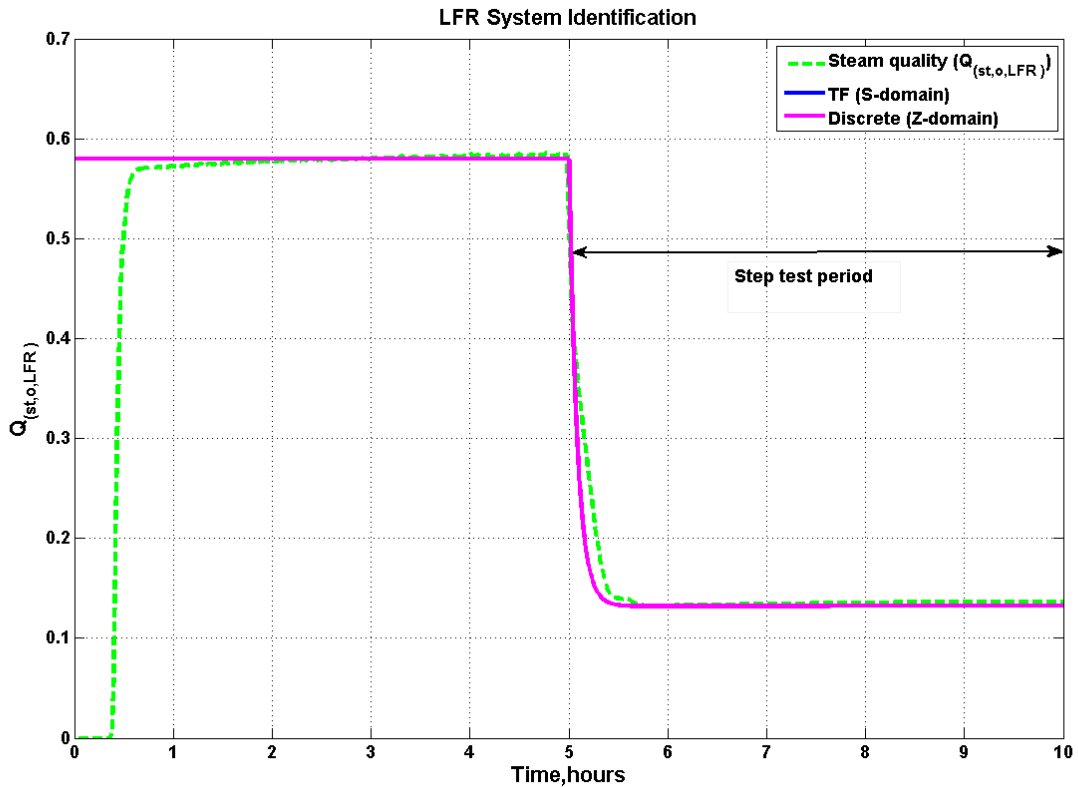


FIGURE 6. LFR system identification.

TABLE 5. PI controller tuning rules.

G_P	G_{CL}	K_C	τ_I
$\frac{K_P}{\tau s + 1}$	$\frac{\gamma s + 1}{\lambda s + 1}$	$\frac{2\tau - \lambda}{K_P \lambda}$	$\frac{2\tau \lambda - \lambda^2}{\tau_P}$

B. LINEAR FRESNEL REFLECTOR (LFR)

The first-order linear transfer function of LFR is obtained by choosing the mass flow-rate of water through LFR ($\dot{m}_{(o,i,LFR)}$), and the quality of steam flow out of LFR ($Q_{(st,o,LFR)}$) as the manipulated and control variable, respectively.

In this step test solar radiation ($I = 200\text{w}/\text{m}^2$) and the temperature of water flow into LFR ($T_{(w,i,LFR)} = 35^\circ\text{C}$) is also maintained. While performing the step test, the remaining certain input parameters are kept constant for LFR, parameters are shown in Table 4.

LFR’s first-order model is obtained for the continuous and discrete system by comparing the fitted transfer function of LFR with the steam quality, as shown in equation 7 and in Figure 6. Based on the tolerance value (Tol_{TF}) of 1.22 for the 4-hour operation of the step test, the parameters of the transfer function are fixed.

Simulation of LFR under the open-loop and closed-loop is started with initial conditions for an inlet pressure of water flowing in, the temperature of the water flow into LFR ($T_{(w,i,LFR)}$) and water flow rate are maintained at 45 bar,

35°C and 2.4 kg/s respectively. Gridpoint computation of the total length of LFR is converted with grid points of 24000($480 \times 50 = 24000$) [28]. LFR is simulated using numerical scheme obtained using the chatoorgoon model with time interval 60 seconds as discussed in appendix section A.2.

V. CONTROLLER DESIGN

An appropriate controller is opted based on the process model and environmental conditions of the process. Controller tuning should be able to adapt to the uncertainty of model parameters. The continuous form of the PID controller is designed and compared to the design of the discrete form of the digital PFC controller. These two optimal controllers are selected for solar collectors and their performance is compared.

A. PID CONTROLLER

The controller design for dynamic characteristics of solar collectors is obtained using the velocity form of the PI controller, the tuning parameters of PI are obtained based on values as shown in Table 5. In this form of the controller design, the

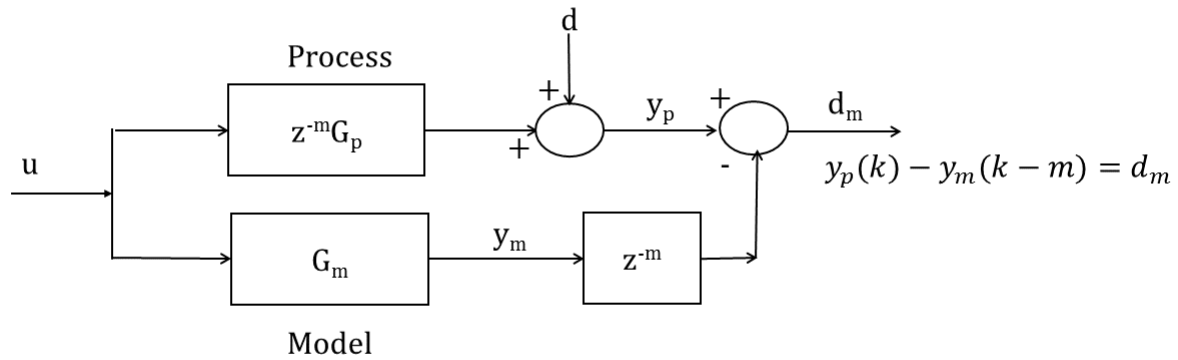


FIGURE 7. Block diagram of PFC.

process error (e) is obtained based on the difference in the control variable and setpoint from the obtained process error manipulated variable (u) which is computed and applied to the actuator of process. By assigning the value of ($\tau_d = 0$) in equation 10, the PID controller can be obtained and implemented as the PI controller.

Velocity form of PID controller:

$$u(k) = q_0 * e(k) + q_1 * e(k - 1) + q_2 * e(k - 2) + u(k - 1)$$

Where $q_0 = K_p(1 + \frac{\tau_d}{T_o})$;

$$q_1 = -K_p * (1 - \frac{T_o}{\tau_i} + 2 * \frac{\tau_d}{T_o}); q_2 = K_p(\frac{\tau_d}{T_o}) \quad (10)$$

Detailed computation of the control algorithm ($u(k)$) of the velocity form of the PI controller is shown in appendix B.

B. PREDICTIVE FUNCTIONAL CONTROL

Predictive Functional Control (PFC) is preferred as the controller since it is simple in coding, computation, tolerating certain values of plant uncertainty, and the dead time of the system and controller can handle the rate of change of input based on the physical constraint.

The basic working principle of PFC [35] is based on future control input (u_k), which is kept constant. Input is chosen such that prediction of the output process (y_p) matches the reference target trajectory (r) at a single point, and repeatedly matches the prediction at a single point within the prediction step (n_p). The model output (y_m) and process output (y_p) minimized by difference value (d_m) as shown in Figure 7.

The control signal for delay model is obtained as:

$$\begin{aligned} & (r - y_m(k) - y_p(k) + y_m(k - m))(1 - \lambda^n) \\ &= b \frac{(1 - a^n)}{1 - a} u(k) + (a^n - 1)y_m(k) \\ & u(k) \\ &= \frac{(r - y_m(k) - y_p(k) + y_m(k - m))(1 - \lambda^n) - (a^n - 1)y_m(k)}{b \frac{(1 - a^n)}{1 - a}} \end{aligned} \quad (11)$$

Detailed computation of the control algorithm ($u(k)$) of PFC obtained in the equation above is shown in appendix B-1.

Implementation of the PFC controller for PTC and LFR consists of inbuilt characteristics of the saturation limit and the rate of change of MV, so that the controller implementation is made simpler as shown in Figure 12.

C. STATIC FEED FORWARD CONTROL

1) STATIC FEED FORWARD CONTROL OF PTC

Static Feed Forward control (SFF) is obtained based on the energy balance of the oil resultant as shown in Equation 12. Furthermore, it is combined with the feedback control of the PI control System and the resultant manipulated variable for PTC ($\dot{m}_{(o,i,PTC)} = \dot{m}_{(o,FF)} + u_k$) is obtained as shown in Figure 8.

$$\begin{aligned} \dot{m}_{(o,FF)}(h_{(o,o,PTC)} - h_{(o,i,PTC)}) &= IA\eta_{(opt,PTC)} \\ \dot{m}_{(o,FF)} &= \frac{IA\eta_{(opt,PTC)}}{(h_{(o,o,PTC)} - h_{(o,i,PTC)})} \end{aligned} \quad (12)$$

2) STATIC FEED FORWARD CONTROL OF LFR

Static Feed Forward control (SFF) is obtained based on the energy balance of enthalpy of the two-phase mixture resultant, which is shown in Equation 13, and combined with the feedback control of the PI control system, and then determining the resultant manipulated variable for LFR ($\dot{m}_{(w,i,LFR)} = \dot{m}_{(w,i,FF)} + u_k$), which is obtained as shown in Figure 13.

$$\begin{aligned} (\dot{m}_{(st,o)}h_{(st,o)} + \dot{m}_{(w,o)}h_{(w,o)}) - (\dot{m}_{(w,i)}h_{(w,i)}) &= (IA\eta_{(opt,LFR)}) \\ \dot{m}_{(w,i,FF)} \\ &= - \left[\frac{(IA\eta_{(opt,LFR)}) - (\dot{m}_{(st,o)}h_{(st,o)}) - (\dot{m}_{(w,o)}h_{(w,o)})}{h_{(w,i)}} \right] \end{aligned} \quad (13)$$

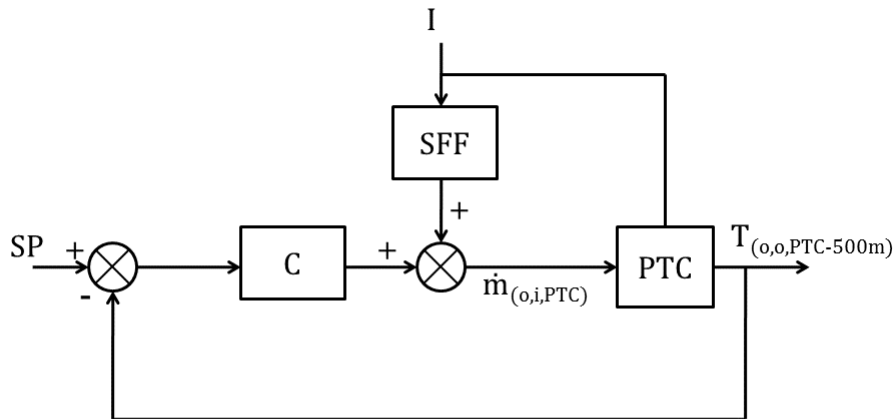
The transient response of the solar collector evaluates the performance of the controller in a closed-loop operation based on the cost value obtained as shown in Table 6.

VI. CLOSED LOOP CONTROLLER DESIGN FOR SOLAR COLLECTORS

In a solar thermal power plant, load demands vary depending on climate conditions and the time period. Operating solar collectors requires efficiency and safety which is a major task. Using the individual control loop of solar collectors operating

TABLE 6. Controller performance indicator.

Cost function	
Integral Absolute Error (IAE)	$\int_0^\infty e_{rr} dt$
Integral Squared Error (ISE)	$\int_0^\infty e_{rr}^2 dt$
Integral Time Absolute Error (ITAE)	$\int_0^\infty t e_{rr} dt$
Integral Time Squared Error (ITSE)	$\int_0^\infty te_{rr}^2 dt$



SP = Set Point C= Controller $\dot{m}_{(o,i,PTC)}$ = Mass flow rate of oil towards PTC

SFF = Static Feedward Control $T_{(o,o,PTC-500m)}$ = Temperature of oil at PTC at 500m

FIGURE 8. PTC PI-control system block diagram.

within their physical constraints, the entire hybrid STP can be controlled within physical reliability.

The performance of solar collectors is analyzed with two inputs, a constant input and a varying input. Based on these two inputs, six case studies were performed as listed below. (1) Constant Input open-loop operation (C-open) (2) varying Input open-loop operation (V-open) (3) constant input with PI and static feed-forward control (C-PI) (4) varying input with PI and static feed-forward control (V-PI) (5) constant input with PFC control (C-PFC) (6) varying input with PFC control (V-PFC). The first two case studies (C-open, V-open) were used to compare the controller performance in the closed-loop operation. Robustness of controller performance on solar collectors (PTC and LFR) is tested by varying set point at 2 and 4 hours operation its performance metric on above case studies is shown in Appendix C.

A. CONTROLLER DESIGN FOR PARABOLIC TROUGH COLLECTOR

The focus of PTC towards solar radiation is a major task. Solar radiations are difficult to predict due to cloud cover and variations in temperature of oil coming in towards the PTC, which are disturbances that affect the output of thermal energy gained in PTC.

A schematic of disturbance and the manipulated control variable is shown in Figure 4. Furthermore, these are highlighted in Table 4. In addition, the control loop structure is shown in Figure 8. The control variable for PTC is used to control the outlet oil temperature of PTC ($T_{(o,o,PTC)}$) by manipulating the oil flow rate through PTC ($\dot{m}_{(o,o,PTC)}$).

Variation of the manipulated variable of PTC ($\dot{m}_{(o,o,PTC)}$) affects parameters as shown below.

- During the disturbance solar period, thermal stress variation occurs in the PTC receiver tube. This variation should be within the feasible limit for long-term PTC operation.
- The control loop operation of PTC, which increases the gain in thermal energy $T_{(o,o,PTC)}$, follows a similar pattern as the solar radiation, whereas $\dot{m}_{(o,i,PTC)}$ responds with reverse behavior compared to solar radiation.
- The heat transfer coefficient increases with thermol oil when the oil flow is increased and is reduced for low oil flow rate.
- When $T_{(o,o,PTC)}$ is high, it takes less time to initiate electric power generation (POW_{ele}), and POW_{ele} generation is extended depending on its sustainability.

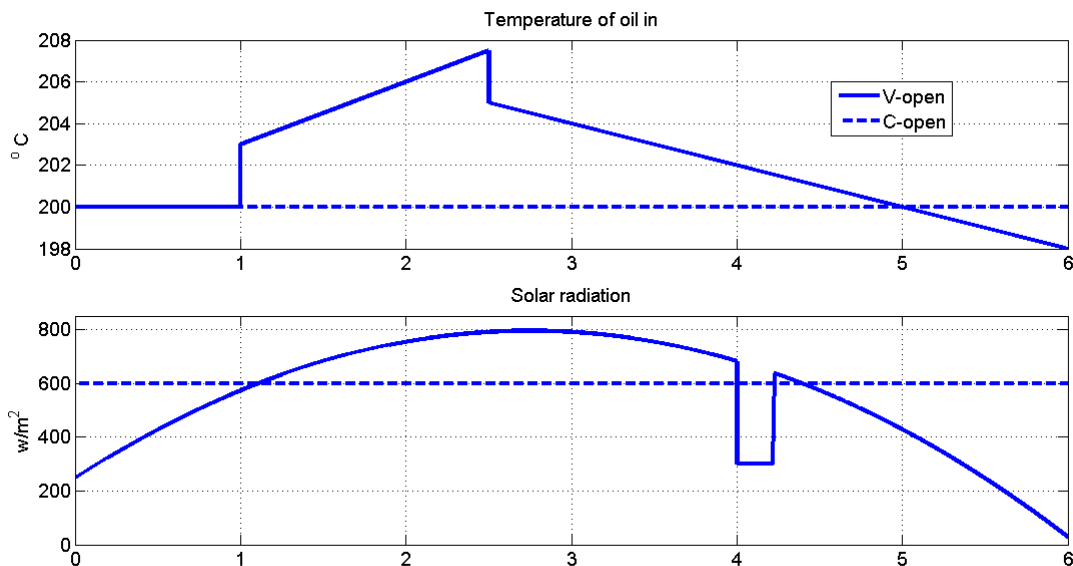


FIGURE 9. PTC input parameters for simulation.

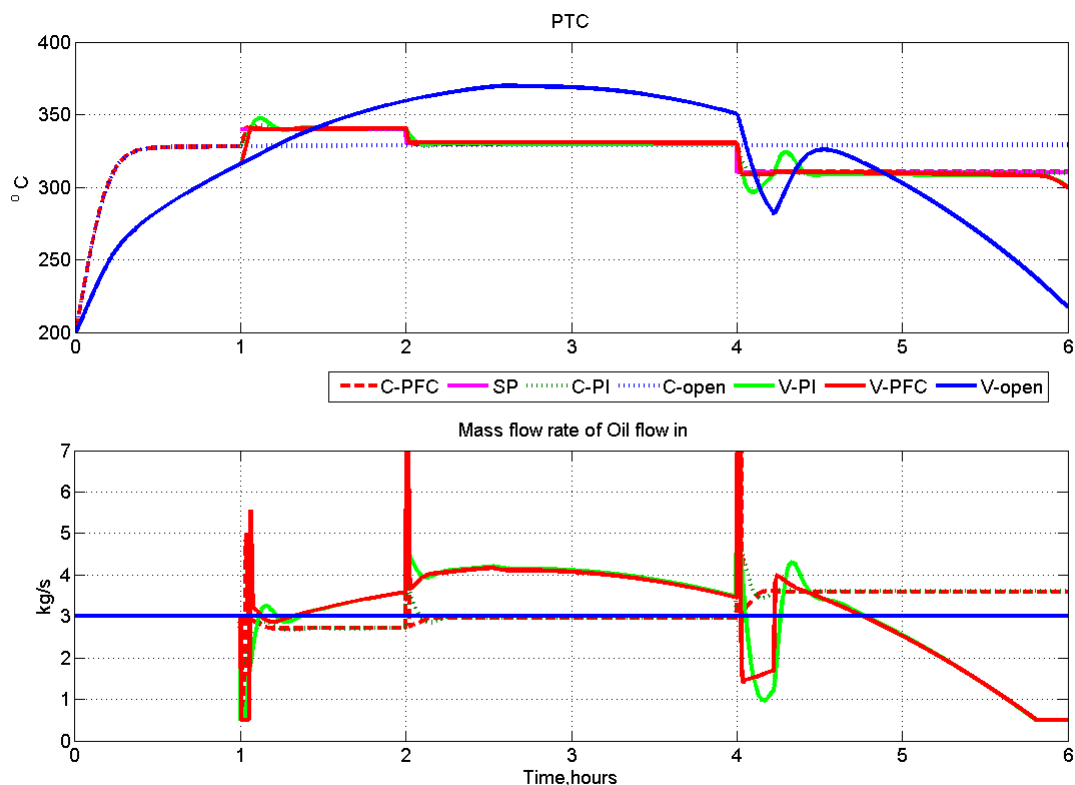
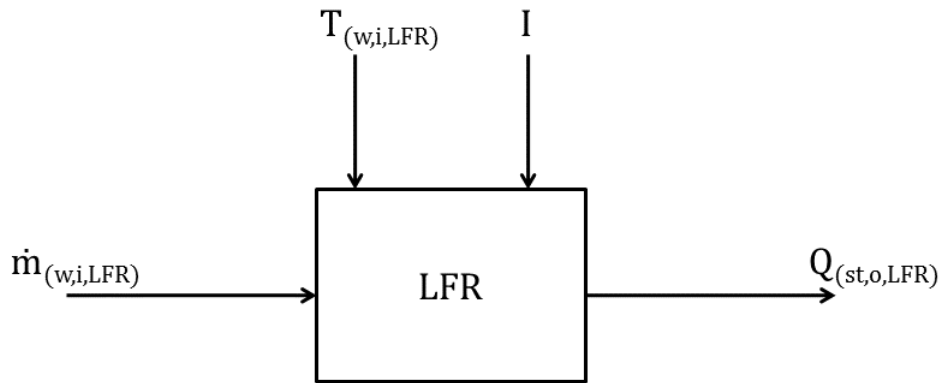


FIGURE 10. Profile of PTC.

Inputs applied to evaluate the performance of PTC with the closed-loop controller are shown in Figure 9. The performance of controllers assessed based on the case studies are stated in chapter VI. Since in the open-loop operation of the case studies (C-open, V-open) the manipulated variable is

kept constant, the oscillation of MV is absent. The optimal controller is selected based on the two criteria of cost value obtained, and oscillation of the manipulated variable. For the PFC controller, the maximum variation of the oil flow rate ($\dot{m}_{(o,o,PTC)}$) per second is maintained only by 0.5 kg/s,



$\dot{m}_{(w,i,LFR)}$ = Mass flow rate of water in towards LFR

$T_{(w,i,LFR)}$ = Temperature of water in towards LFR

$Q_{(st,o,LFR)}$ =Quality of steam flow out of LFR

I =Solar radiation

FIGURE 11. LFR control parameters.

as shown in Figure 10. Based on these criteria, the PFC controller presents a better performance compared to the PI closed-loop controller relative to the set point and disturbance rejection.

Different case studies were performed for PTC variation of the control variable ($T_{(o,o,PTC)}$) because it is a critical parameter, and should be maintained within the limits to avoid thermal stress in the PTC receiver tube. During the disturbance solar period ranging from 4 hour to 4.15 hour, the thermal stress variation is highlighted in these studies. Considering the different case studies, a varying input causes greater variation compared to constant inputs; a variation of $T_{(o,o,PTC)}$ reduces by approximately 19%, 10%, and 6% for the case studies with the conditions of varying input open-loop (V-open), varying input PI (V-PI), and varying input PFC (V-PFC), respectively, as shown in Figure 6.

B. CONTROLLER DESIGN FOR LINEAR FRESNEAL REFLECTOR

The focus of LFR towards solar radiation is a major task. Solar radiation is difficult to predict due to cloud cover and variations in temperature of water flowing in towards the LFR, which are disturbances that affect the output of thermal energy gained in LFR.

A schematic of disturbance, manipulated, and control variable is shown in Figure 4. Furthermore, these are highlighted in Table 4. In addition, the control loop structure is shown in Figure 8. The control variable for LFR is used to control

the quality of steam flowing out of the LFR ($Q_{(st,o,LFR)}$) by manipulating the oil flow rate through PTC ($\dot{m}_{(w,i,LFR)}$). Variation of a manipulated variable of LFR ($\dot{m}_{(w,i,LFR)}$) affects parameters as shown below:

- In LFR operation, thermal stress causes a severe problem in LFR similar to PTC, and variation in the temperature of water (or) two-phase flow also needs to be monitored within the limits. Subsequently, temperature variation causes vibrations in the LFR pipe due to pressure variation.
- Consistent steam generation from DSG is obtained by varying the flow rate of water into the LFR, enabling the mass of steam production generated from the LFR and SD to directly drive the turbine.
- The temperature and pressure of water in the SD are affected, reducing the input thermal energy to LFR.

The performance of LFR in open and closed-loop operation is shown in Figure 14. The performance of the open-loop operation of LFR with a constant and varying input is tested; the manipulated variable is kept constant, but the variation of quality of steam from the LFR and the pressure variation along LFR is shown in Figure 15. Because the variation of pressure can cause a vibration in LFR, it is monitored and needs to be maintained within a limit compared to steam production. The performance of the manipulated variable ($\dot{m}_{(w,i,LFR)}$) optimizes the variation by maintaining a maximum change of water flow into LFR at 4.8 kg/s. Based on the variation performance of the manipulated variable criteria, PFC could be preferred compared to the PI controller.

PFC= Predictive Functional Control

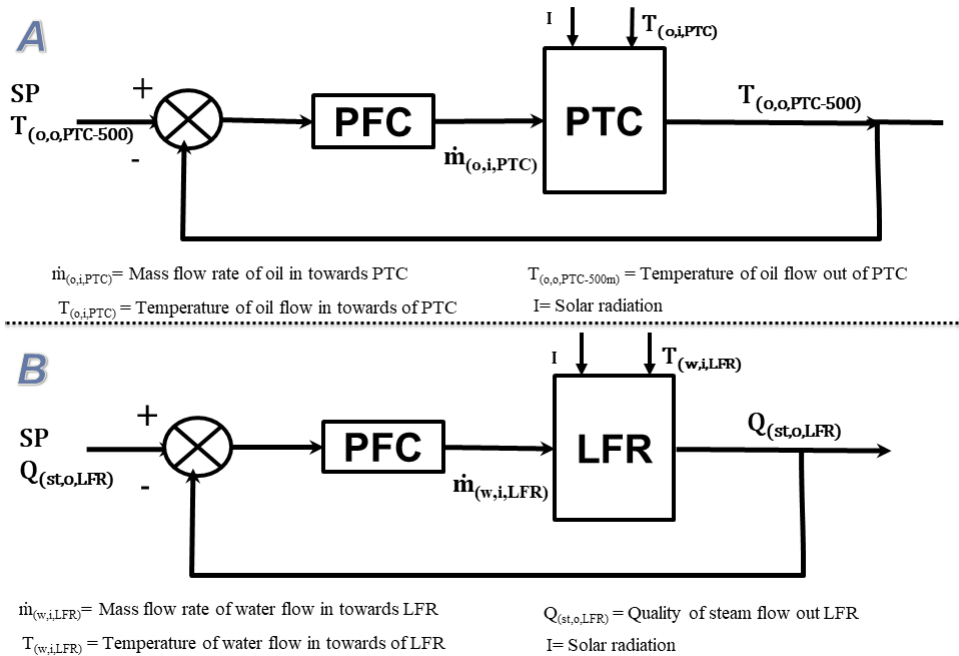
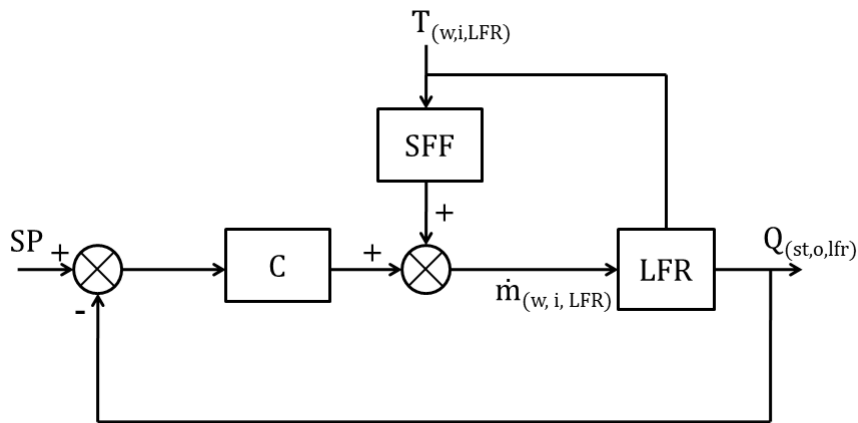


FIGURE 12. (a) PFC controller for PTC (b) PFC controller for LFR.



$\dot{m}_{(w,i,LFR)}$ = Mass flow rate of water in towards LFR
 $T_{(w,i,LFR)}$ = Temperature of water in towards LFR
 $Q_{(st,o,LFR)}$ = Quality of steam flow out of LFR
 I = Solar radiation
 C = Controller
 SFF = Static Feedforward Controller

FIGURE 13. PI-control block diagram of LFR.

Whereas considering steam quality ($Q_{(st,o,LFR)}$) as the control variable constraint, the PI controller with a static feed-forward controller is preferred.

Controlling steam quality flow out of LFR ($Q_{(st,o,LFR)}$) needs to be maintained within limits, which can otherwise

cause thermal stress on LFR tubes and subsequent pressure variation due to the vibration in the LFR tubes. During solar radiation disturbance, the control and the manipulated variable are analyzed. Case studies of conditions with varying input open-loop (V-open), varying input PI(V-PI), and

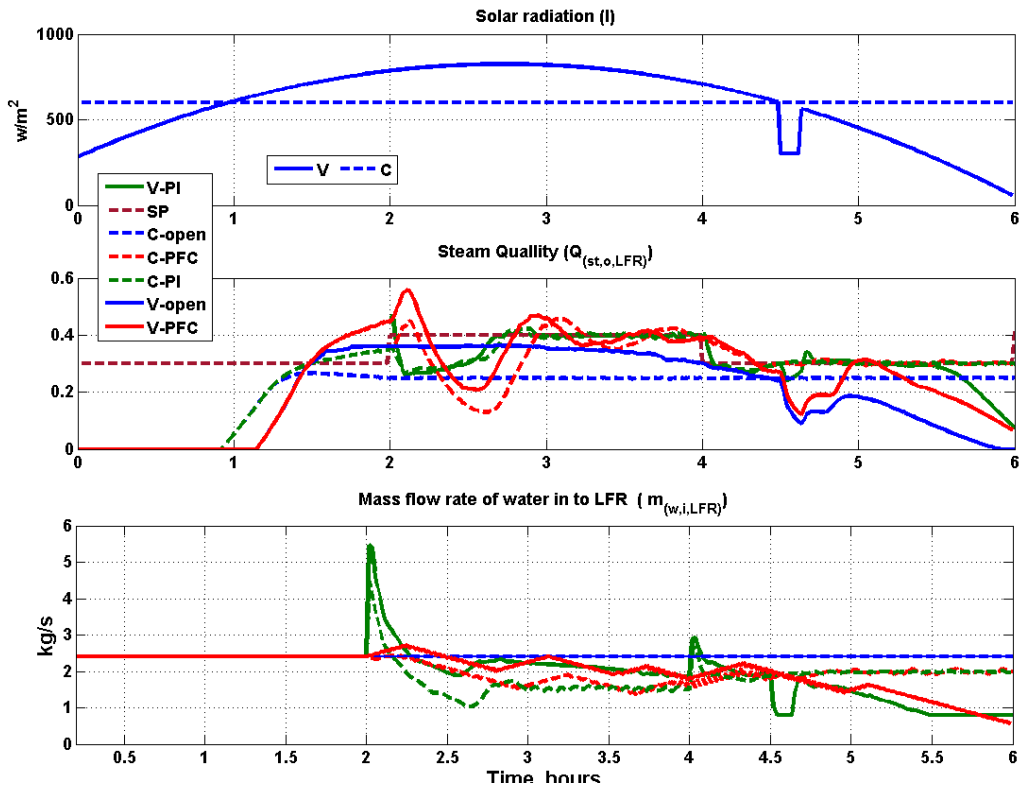


FIGURE 14. Profile of LFR.

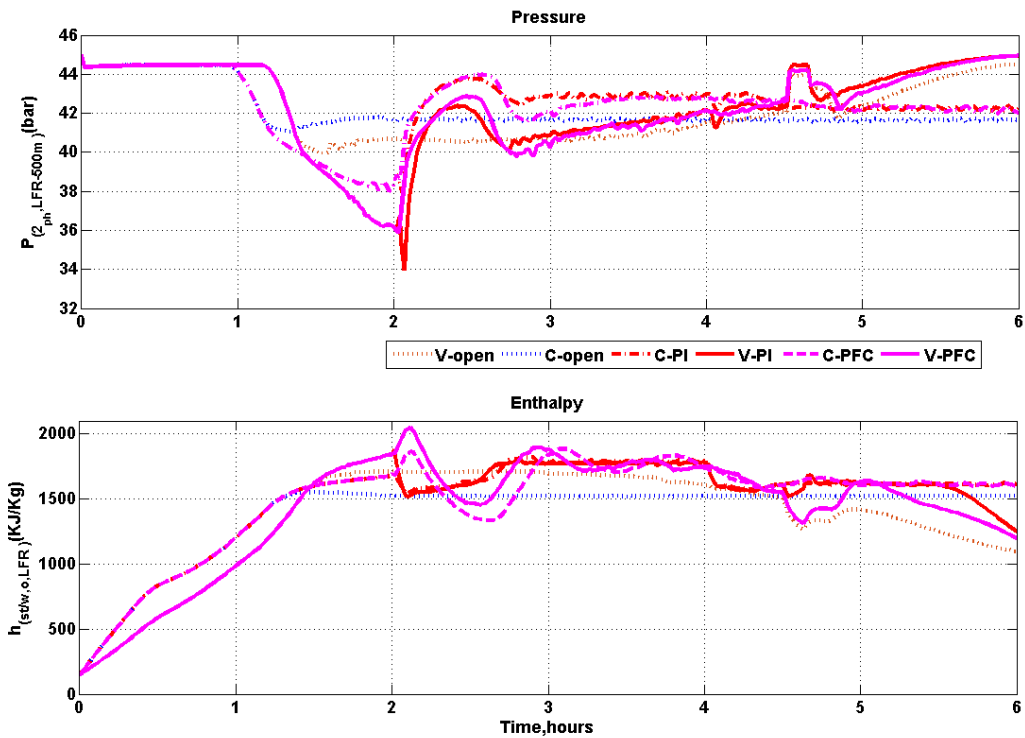


FIGURE 15. Pressure and enthalpy profile of LFR.

varying input PFC (V-PFC) control variable ($Q_{(st,o,LFR)}$) reduce the values by 60%, 55%, and 17.6%. However, the manipulated variable ($\dot{m}_{(w,i,LFR)}$) increases by approximately

50%, 13%, and 54%, respectively. Considering the simulation studies of LFR above, the manipulation varies drastically in the PI controller.

VII. CONCLUSION

Solar collectors with therminol oil-based and direct steam generation-based nonlinear processes are analyzed in this study. Both processes are analyzed by the comparison of an open and closed-loop operation with constant and varying inputs. A fitted transfer model based on continuous and discrete functions is obtained from the first principle model; tuning of the controller is obtained based on the IMC tuning for a continuous-time controller design, and is added with balance static feed-forward control using energy balance. The PFC control design is also based on the first-order discrete model. Considering these two controllers, a physical reliable controller was opted based on the manipulated oscillation for set-point tracking and disturbance rejection. The performance of the PI controller with SFF shows satisfactory performance for PTC and LFR. During solar radiation for a disturbance at 4 hours, maximum deviation from setpoint are obtained 9° C for variable input PI Controller design with recovery period about 24 minutes, whereas in other case study and controller implementation it is less than 2° C with a recovery time of maximum 2 minutes. PFC controller also shows a similar satisfactory performance overtime period. During solar radiation for a disturbance at 4 hours 30 minutes, maximum deviation from setpoint are obtained about 0.28 for variable input PFC Controller design with recovery period about 30 minutes but MV changes only by 2.04 to 1.88 kg/s. with other controller implementation on case studies, it has a maximum deviation from the setpoint is about 0.06 during the solar radiation disturbance period. The proposed digital-type PFC controller is opted based on the cost function and the variation rate of change in the manipulated variable.

APPENDIXES

APPENDIX A DETAIL MODELING OF LINEAR FRESNEL REFLECTOR

In this section, modeling of the Linear Fresnel Reflector (LFR) [28] is discussed for equations (2a)-(3b) of the main article.

The dynamic behavior of LFR is studied by solving the time dependent mass, momentum, and energy conservation equations representing the system. These governing equations, which form a system of non-linear equations, are solved numerically using Chatoorgoon's (1986) approach [33]. Assumptions made in the model are listed below:

- 1) Flow is assumed to be one dimensional.
- 2) Two-phase homogeneous flow is considered.
- 3) There is no slip between liquid and steam flow.
- 4) Maximum pressure drop is known initially, to enable computation of min/max time step size.

Chatoorgoon's Model [33] is preferred for the dynamic modeling of LFR. This modeling approach consists of three important advantages: (1) Property derivatives are not used, (2) Inversion of matrices is not needed, and (3) Small or large time steps can be used.

The liquid properties for the entire length of the pipe are computed by discretizing functions and solving the mass, energy, and momentum equations using the average properties in each section. These equations are solved implicitly.

A. DYNAMIC MODELING OF LFR

Dynamic simulation of LFR is obtained using Chatoorgoon's model. In the energy equation (16), q_w represents the heat supplied from solar energy. The dynamic model of LFR consists of the following equations derived from the first principles as [33]:

$$\text{Mass: } \frac{\partial \rho}{\partial t} + \frac{\partial(\rho u)}{\partial x} = 0 \quad (14)$$

$$\text{Momentum: } \frac{\partial(\rho u)}{\partial t} + \frac{\partial(\rho u^2)}{\partial x} + \frac{\partial P}{\partial x} + C_k \rho u^2 + \rho g = 0 \quad (15)$$

$$\text{Energy: } \frac{\partial}{\partial t} \left[\left(\rho \left(h + \frac{u^2}{2} \right) \right) \right] + \frac{\partial}{\partial x} \left[\left(\rho u \left(h + \frac{u^2}{2} \right) \right) \right] + \rho u g = \frac{\partial P}{\partial t} + q_w \quad (16)$$

$$\text{State: } \rho = f(P, h) \quad (17)$$

Discretization of mass, momentum, and energy equations (14 to 16) is explained in detail below. The discretization scheme is taken from Chatoorgoon (1986) [33] and is reproduced here for completeness. Additionally, discretization is also performed for the absorber pipe and the glass envelope to obtain the complete LFR model. In the equations that follow, the subscript i represents the grid point, and the superscript n represents the time index.

By discretizing the mass equation (3a), we obtain :

$$\frac{\Delta x}{2} \frac{d}{dt} [\rho_i + \rho_{i+1}] + (\rho u)_{i+1}^{n+1} - (\rho u)_i^{n+1} = 0$$

$$\text{Further, using } \frac{d\rho_i}{dt} = \frac{\rho_i^{n+1} - \rho_i^n}{\Delta t}, \text{ we obtain}$$

$$\frac{\Delta x}{2\Delta t} \left[(\rho_i^{n+1} + \rho_{i+1}^{n+1}) - (\rho_i^n + \rho_{i+1}^n) \right] + (\rho u)_{i+1}^{n+1} - (\rho u)_i^{n+1} = 0$$

$$\Rightarrow \left[\frac{\Delta x}{2\Delta t} + u_{i+1}^{n+1} \right] \rho_{i+1}^{n+1} + Q^n + R_i = 0$$

$$\text{where, } Q^n = \frac{-\Delta x}{2\Delta t} [(\rho_i^n + \rho_{i+1}^n)]$$

$$\text{and } R_i = \left(\frac{\Delta x}{2\Delta t} - u_i^{n+1} \right) \rho_i^{n+1} \quad (18)$$

By discretizing the momentum equation (15), we obtain:

$$\rho_{i+1}^{n+1} + \rho_{i+1}^{n+1} \left(g \frac{\Delta x}{2} + \theta_u \left(1 + C_k \frac{\Delta x}{2} \right) \right) (u^2)_{i+1}^{n+1} + \frac{\Delta x}{2\Delta t} (u)_{i+1}^{n+1} + S^n + T_i = 0 \quad (19)$$

Where, $0 \leq \theta_u \leq 1$,

$$S^n = \frac{-\Delta x}{2\Delta t} ((\rho u)_{i+1}^n + (\rho u)_i^n) + (1 - \theta_u) \times \left[(\rho u^2)_{i+1}^n (1 + C_k \frac{\Delta x}{2}) - (\rho u^2)_i^n (1 - C_k \frac{\Delta x}{2}) \right]$$

$$+g \frac{\Delta x}{2} [(\rho_{i+1}^n + \rho_i^n)],$$

and $T_i = \left(\frac{\Delta x}{2\Delta t} (\rho u)_i^{n+1} \right)$

$$+ \theta_u \left[g \frac{\Delta x}{2} \rho_i^{n+1} - \left(1 - C_k \frac{\Delta x}{2} \right) - (\rho u^2)_i^{n+1} \right] - P_i^{n+1}$$

By discretizing the Energy equation (16), we obtain:

$$\left[h_{i+1}^{n+1} + \frac{(u_{i+1}^2)^{n+1}}{2} \right] \left((\rho u)_{i+1}^{n+1} + \frac{\Delta x}{2\Delta t} \rho_{i+1}^{n+1} \right) + g \frac{\Delta x}{2} (\rho u)_{i+1}^{n+1} - \frac{\Delta x}{2\Delta t} P_{i+1}^{n+1} + y^i + W_i = 0 \quad (20)$$

with, $y^i = -\frac{\Delta x}{2\Delta t} \left[\rho_{i+1}^n \left(h_{i+1}^n + \left(\frac{u_{i+1}^2}{2} \right)^n \right) + \rho_i^n \left(h_i^n + \left(\frac{u_i^2}{2} \right)^n \right) - P_{i+1}^n - P_i^n \right]$

$$W_i = \frac{\Delta x}{2\Delta t} \left[\rho_i^{n+1} \left(h_i^{n+1} + \left(\frac{u_i^2}{2} \right)^{n+1} \right) - P_i^{n+1} \right] - (\rho u)_i^{n+1} \left(h_i + \frac{u_i^2}{2} \right)^{n+1} + g \frac{\Delta x}{2} (\rho u)_i^{n+1} - q_w \Delta x,$$

Energy balance for the LFR absorber pipe is obtained as follows:

$$\rho_A C_{AA} A \frac{\partial T_A}{\partial t} = h_p p_{Ai} (T_{(w/st/2\phi)} - T_A) - \frac{\sigma}{\frac{1}{\xi A} + \frac{1-\xi_E}{\xi E} \left(\frac{T_A}{T_E} \right)} p_{Ao} (T_A^4 - T_{sky}^4) + I_c \eta_{opt} W - h_{air} p_{Eo} (T_A - T_{air}) \quad (21)$$

This energy balance equation is discretized as:

$$T_{A,i+1}^{n+1} = \frac{1}{\rho_A C_{AA} A} \left(h_p p_{Ai} (T_{(w/st/2\phi,i)^{n+1}} - T_{A,i}^{n+1}) - \frac{\sigma}{\frac{1}{\xi A} + \frac{1-\xi_E}{\xi E} \left(\frac{T_{A,i}^{n+1}}{T_{E,i}^{n+1}} \right)} p_{Ao} ((T_{A,i}^{n+1})^4 - T_{sky}^4) + I_c \eta_{opt} W - h_{air} p_{Eo} (T_{A,i}^{n+1} - T_{air}) \right)$$

where, $T_{A,i}^{n+1}, T_{E,i}^{n+1}$ represents the temperatures of the absorber and glass pipe, respectively, in the grid cell i at time index $n + 1$.

Energy balance for the LFR glass envelope is obtained as follows:

$$\rho_E C_{EA} E \frac{\partial T_E}{\partial t} = \frac{\sigma}{\frac{1}{\xi A} + \frac{1-\xi_E}{\xi E} \left(\frac{T_A}{T_E} \right)} p_{Ai} (T_A^4 - T_E^4) - \sigma p_{Eo} \xi_E (T_E^4 - T_{sky}^4) - h_{air} p_{Eo} (T_E - T_{air}) \quad (22)$$

which upon discretization yields,

$$T_{E,i+1}^{n+1} = \frac{1}{\rho_E C_{EA} E} \left(\frac{\sigma}{\frac{1}{\xi A} + \frac{1-\xi_E}{\xi E} \left(\frac{T_{A,i}^{n+1}}{T_{E,i}^{n+1}} \right)} p_{Ai} ((T_{A,i}^{n+1})^4 - (T_{E,i}^{n+1})^4) - \sigma p_{Eo} \xi_E ((T_{E,i}^{n+1})^4 - T_{sky}^4) - h_{air} p_{Eo} (T_{E,i}^{n+1} - T_{air}) \right) \quad (23)$$

The parameter θ_u in the momentum equation (19) multiplies the terms of acceleration and frictional pressure drop. θ_u can theoretically be any value between 0 and 1. If the configuration of the LFR pipe is other than in the horizontal position, then θ_u takes values depending on the angle as measured from the reference position. The term q_w in the energy equation is linked with the solar energy received per unit volume on an absorber pipe for sectional length and is computed as:

$$q_w = \frac{Q_{heat}}{(\pi r_{Ao}^2 \Delta x)}$$

where $Q_{heat} = h_{(p,LFR)} A_A (T_A - T_{(w/st/2\phi)})$ (24)

The heat transfer coefficient $h_{(p,LFR)}$ may be $h_{(p,1\phi)}$ or $h_{2\phi}$ depending on the working fluid condition such as the single phase and two-phase conditions, respectively. The computation of these heat transfer coefficients is discussed in section VII-B.2. Furthermore, $T_{(w/st/2\phi)}$ represents the temperature of the working fluid, Δx is the distance between the two grid points in the finite difference approximation, and Δt is the time step.

Energy conservation equations (14-16) are appended with the absorber pipe and the glass envelope resulting in 5 conservation equations for the LFR; these equations are discretized as presented above. These equations corresponding to a receiver tube length of 480 meters were discretized into 24000 uniform segments using finite backward difference resulting in 120,000 ODEs, with each section length equal to 0.02 m. The number of segments were obtained based on trial and error. The ODEs were again discretized in time by using a forward difference scheme in the time domain as in the equations above.

The time step (Δt) used for time-discretization should satisfy: $\Delta t > \frac{\Delta x}{2a}$ where 'a' is the speed of sound in the two-phase mixture, and Δx is the grid section length. In our study, this corresponds to the requirement that Δt should be greater than 16 milliseconds; approximately the value of the sonic speed computed from Kieffer (1977) [36].

B. SOLUTION ALGORITHM FOR CHATOORGOON MODEL

The solution of discretized mass (equation 18), momentum (equation 19), and energy (equation 20) balance equations involve four unknowns: $\rho_{i+1}^{n+1}, u_{i+1}^{n+1}, P_{i+1}^{n+1}$ and h_{i+1}^{n+1} . The state equation (17) provides the fourth equation. The following iterative procedure is used to obtain the unknowns [33]:

- 1) Initial condition: At $t=0$, all the unknown variables (ρ, u, P, h) are assumed to have the same values at all

grid points. These values are based on the first grid point initial values.

- 2) For a given instant of time $n + 1$, the following procedure is used to obtain the convergence at grid point $i + 1$:
 - a) Guess ρ_{i+1}^{n+1} and then compute u_{i+1}^{n+1} , P_{i+1}^{n+1} , h_{i+1}^{n+1} (using Equations 18,19 and 20 respectively). Compute ρ_{i+1}^{n+1} from the state equation (Equation 17).
 - b) If $|\rho_{i+1}^{n+1} - \rho_{new,i+1}^{n+1}| > \text{tolerance}$, go back to step (a).
- 3) Upon convergence at grid point $i + 1$, increment i and continue the above steps. Since the conditions at the first grid point correspond to the inlet conditions, this procedure can be used to now proceed forward in space.
- 4) Once the entire spatial profile at the time instant $n + 1$ is generated, then increment the time instant and go back to step 2.

Note, during the procedure, if $h_{i+1}^{n+1} < h_{Liquid}^{sat}$ then the single-phase HTC and single-phase friction factor are used. However, if $h_{i+1}^{n+1} > h_{Liquid}^{sat}$ then the two-phase HTC and two-phase friction factor are used.

1) FRICTION COEFFICIENT COMPUTATION [28]

Pipe friction coefficient (f_f) for laminar flow is given by:

$$f_f = \frac{64}{Re}$$

The pipe friction coefficient for turbulent flow is determined using the Reynolds number (Re), pipe roughness (ε), and pipe diameter (D_a) as [37]:

$$\frac{1}{\sqrt{f_f}} = -2 \log_{10} \left(\frac{\varepsilon/D_a}{3.7} + \frac{2.51}{Re \sqrt{f_f}} \right) \quad (25)$$

Equation (25) is an implicit equation in f_f , and is solved iteratively until convergence. The computation of the friction factor (C_k) for Equation (15) is obtained as follows:

$$C_k = \frac{f_f}{2D_a} \quad (26)$$

Single phase viscosity of water is obtained from [38], whereas for the two-phase, viscosity is computed as follows [39]:

$$\frac{1}{\mu_{2\phi}} = \frac{q}{\mu_g} + \frac{1-q}{\mu_L} \quad (27)$$

where $\mu_{2\phi}$ is the two-phase viscosity, and q represents the quality of steam (refer Equation (31)). The viscosity is then used to compute the Reynolds number which is subsequently used in C_k computation.

2) HEAT TRANSFER COEFFICIENT IN DSG [28]

We now discuss the computation of the convective heat transfer coefficient of the working fluid in LFR (water stream) when it is in: (1) Single phase, (2) Twophase, or is (3) Dry steam.

Single phase convective heat transfer coefficient ($h_{p,1\phi}$):

The single phase convective heat transfer coefficient for working fluid is obtained as: [40].

$$h_{p,1\phi} = 0.023 R_e^{0.8} P_r^{0.4} \frac{K}{D_a} \quad (28)$$

where the Reynolds number and Prandtl number are computed as:

$$\text{Reynolds number } R_e = \frac{D_a u}{\nu}, \quad \text{Prandtl number } P_r = \frac{\nu \rho C_p}{K}$$

Two-Phase Heat Transfer Coefficient ($h_{2\phi}$): For two-phase flow boiling, the heat transfer coefficient is studied and analyzed by Odeh *et al.* (1998) [34] and Arousseau *et al.* (2015) [41]. To evaluate the heat transfer coefficient in the two-phase zone, the flow pattern must be determined using the Froude number (Fr) defined as [34], [41]:

$$F_r = \frac{G^2}{\rho_l^2 g D_a}$$

If $F_r < 0.04$ then stratified flow occurs and the heat transfer coefficient is given by the Shah equation [34], [41]:

$$F_r < 0.04 : \quad \frac{h_{2\phi}}{h_1} = 3.9(F_r)^{0.24} \left[\frac{q}{1-q} \right] \left[\frac{\rho_l}{\rho_v} \right]^{0.4} \quad (29)$$

where $h_{2\phi}$ is the two-phase heat transfer coefficient. The heat transfer coefficient for liquid flow (h_1) can be calculated using the Dittus-Boelter equation assuming the liquid fraction fills the tube as:

$$h_1 = 0.023 \left[\frac{k}{D_{ab}} \right] \left[\frac{G(1-q)D_a}{\mu_l} \right]$$

When $F_r > 0.04$, the two-phase heat transfer coefficient ($h_{2\phi}$) has two independent components: Bubble formation (h_B) and convection (h_1) as:

$$\begin{aligned} h_{2\phi} &= h'_B + h'_1 \\ \text{with, } h'_B &= h_B S \\ \text{and } h'_1 &= h_1 F \end{aligned} \quad (30)$$

Further,

$$\begin{aligned} h_B &= 3800 \left(\frac{q}{20,000} \right)^n F_p \\ n &= 0.9 - 0.3(P_n)^{0.15} \\ F_p &= 2.55(P_n)^{0.27} \left(9 + \frac{1}{1 - P_n^2} \right)^{P_n^2} \\ P_n &= P/P_{cr} \\ S &= \frac{1}{1 + (0000015)F^2(R_e)^{1.17}} \\ R_e &= \frac{G(1-q)D_{ab,i}}{\mu_l} \end{aligned}$$

In the above, P_n represents pressure of working fluid, P_{cr} is the critical pressure, and q stands for quality of steam. S and F are Correction and Enhancement factors. F is computed as:

$$F = (1 + 24000)(B_o)^{1.16} + 1.37X_{tt}^{-0.86}$$

where the Boiling number (B_o) and Martinelli parameter (X_{tt}) are computed as:

$$B_o = \frac{q}{Gh_{fg}}$$

$$X_{tt} = \left(\frac{\rho_g}{\rho_l}\right)^{0.5} \left[\frac{\mu_l}{\mu_g}\right]^{0.1} \left[\frac{1-q}{q}\right]^{0.2}$$

The steam quality is computed using the following expression

$$h_{out} = qh_g + (1-q)h_f$$

$$\implies q = \frac{h_{out} - h_f}{h_g - h_f} \quad (31)$$

with h_{out} , h_f , h_g , h_{fg} , and G being the enthalpy of water going out, enthalpy of fluid, enthalpy of steam, latent heat, and mass flux, respectively.

APPENDIX B DETAIL IMPLEMENTATION DIGITAL FORM OF PID / PI CONTROLLER

The general continuous form of a PID controller is given as:

$$u(t) = K_p * [e(t) + \frac{1}{\tau_i} \int e(t)dt + \tau_d * \frac{de(t)}{dt}] \quad (32)$$

Position form of PID controller

$$u(k) = K_p * [e(k) + \frac{T_o}{\tau_i} * \sum_{i=0}^{k-1} e(i) + \frac{\tau_d}{T_o} * (e(k) - e(k-1))] \quad (33)$$

If the current input signal is shifted by time,

$$u(k-1) = K_p * [e(k-1) + \frac{T_o}{\tau_i} * \sum_{i=0}^{k-2} e(i) + \frac{\tau_d}{T_o} * (e(k-1) - e(k-2))] \quad (34)$$

Subtracting the Equation (33) to (34) and resultant change in the input is obtained as $\Delta u(k) = u(k) - u(k-1)$

Velocity form of PID controller

$$\Delta u(k) = K_p * [(e(k) - e(k-1)) + \frac{T_o}{\tau_i} * e(k-1) + \frac{\tau_d}{T_o} * (e(k) - 2 * e(k-1) + e(k-2))]$$

$$\Delta u(k) = q_0 * e(k) + q_1 * e(k-1) + q_2 * e(k-2) \quad (35)$$

Where $q_0 = K_p(1 + \frac{\tau_d}{T_o})$;

$$q_1 = -K_p * (1 - \frac{T_o}{\tau_i} + 2 * \frac{\tau_d}{T_o}); q_2 = K_p(\frac{\tau_d}{T_o})$$

The velocity form of the PI controller is implemented based on equation 35, the derivative term involved in the equation is ($\tau_d = 0$) eliminated. The above Velocity form of the PID controller has an advantage of no integral windup problems, which protects it from computer failure. Furthermore, it does not need to know the current value of U. Several tuning algorithms are available to control the system based on the FO model.

TABLE 7. Performance metric for PTC.

PTC	IAE	ISE	ITAE	ITSE
Constant PI (C-PI)	7800	1.15 × 10 ⁵	2.27 × 10 ⁷	3.82 × 10 ⁸
Vary PI (V-PI)	1.35 × 10 ⁴	1.34 × 10 ⁵	5.33 × 10 ⁷	4.20 × 10 ⁸
Constant PFC (C-PFC)	1.06 × 10 ⁴	1.12 × 10 ⁵	5.49 × 10 ⁷	3.98 × 10 ⁸
Vary PFC (V-PFC)	9.81 × 10 ⁴	1.188 × 10 ⁵	3.88 × 10 ⁷	3.69 × 10 ⁸

1) PFC WITH DELAY MODEL

The predictive functional control law for the delay model is unbiased, and the undelayed predicted output tracks the target.

Prediction of Model (n-step ahead) is obtained as:

$$y_m(k+n) + d_m = y_{pm}(k+n) = \mathbf{E}[y_p(k+m+n)]$$

$$y_{pm}(k+n) = b \frac{(1-a^n)}{1-a} u(k) + a^n y_m(k) + (y_p(k) - y_m(k-m)) \quad (36)$$

Target selection with discrete pole (λ) is obtained as:

$$r(k+n) = \mathbf{E}[y_p(k+m)] + (r - \mathbf{E}[y_p(k+m)])(1 - \lambda^n)$$

where $y_m(k) + d_m = \mathbf{E}[y_p(k+m)]$;

$$y_p(k) - y_m(k-m) = d_m$$

$$r(k+n) = y_m(k) + d_m + (r - y_m(k) - d_m)(1 - \lambda^n)$$

$$r(k+n) = y_m(k) + y_p(k) - y_m(k-m) + (r - y_m(k) - y_p(k) + y_m(k-m))(1 - \lambda^n) \quad (37)$$

Equating the target and prediction equation:

$$y_m(k) + y_p(k) - y_m(k-m) + (r - y_m(k) + y_p(k) + y_m(k-m))(1 - \lambda^n)$$

$$= b \frac{(1-a^n)}{1-a} u(k) + a^n y_m(k) + (y_p(k) - y_m(k-m)) \quad (38)$$

The control signal for delay model is obtained as:

$$(r - y_m(k) - y_p(k) + y_m(k-m))(1 - \lambda^n)$$

$$= b \frac{(1-a^n)}{1-a} u(k) + (a^n - 1)y_m(k)$$

$$u(k) = \frac{(r - y_m(k) - y_p(k) + y_m(k-m))(1 - \lambda^n) - (a^n - 1)y_m(k)}{b \frac{(1-a^n)}{1-a}} \quad (39)$$

APPENDIX C CONTROLLER PERFORMANCE METRIC FOR CASE STUDIES

From the Figures 10 and 14, observed that the setpoint of PTC and LFR are updated at 2 and 4 hours in all control case studies discussed. Since the setpoint is varied at 2 and 4 hours of PTC and LFR, the control variable during the transition

TABLE 8. Performance metric for LFR.

LFR-Steam quality	IAE	ISE	ITAE	ITSE
Constant PI (C-PI)	324	27	8.25×10^5	0.38×10^5
Vary PI (V-PI)	510	55	35×10^5	4.1×10^5
Constant PFC (C-PFC)	667	106	21×10^5	2.38×10^5
Vary PFC (V-PFC)	1106	145	87×10^5	12×10^5

period are also taken into account for performance metric computation. Table 7 and 8 show the performance metric for PTC and LFR, respectively.

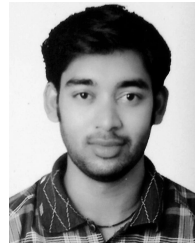
REFERENCES

- [1] N. Bokde, A. Feijóo, D. Villanueva, and K. Kulat, "A review on hybrid empirical mode decomposition models for wind speed and wind power prediction," *Energies*, vol. 12, no. 2, p. 254, 2019.
- [2] (2010). *The Earth Observatory, EOS Project Science Office, NASA Goddard Space Flight Center*. Article on Global Warming. Accessed: Sep. 2018. [Online]. Available: <https://earthobservatory.nasa.gov/features/>
- [3] *United States Environmental Protection Agency Understanding Global Warming Potentials*. Accessed: Oct. 2019. [Online]. Available: <https://www.epa.gov/ghgemissions/understanding-global-warming-potentials>
- [4] N. Bokde, B. Tranberg, and G. Bruun Andresen, "Short-term CO2 emissions forecasting based on decomposition approaches," 2020, *arXiv:2003.10868*. [Online]. Available: <http://arxiv.org/abs/2003.10868>
- [5] J. Hansen, M. Sato, P. Kharecha, D. Beerling, R. Berner, V. Masson-Delmotte, M. Pagani, M. Raymo, D. L. Royer, and J. C. Zachos, "Target atmospheric CO2: Where should humanity aim?" 2008, *arXiv:0804.1126*. [Online]. Available: <http://arxiv.org/abs/0804.1126>
- [6] S. P. Sukhatme and J. Nayak, *Solar Energy*. New York, NY, USA: McGraw-Hill, 2017.
- [7] S. A. Kalogirou, "Solar thermal collectors and applications," *Prog. Energy Combustion Sci.*, vol. 30, no. 3, pp. 231–295, 2004.
- [8] M. H. Alsharif, K. Yahya, and Z. W. Geem, "Strategic market growth and policy recommendations for sustainable solar energy deployment in South Korea," *J. Electr. Eng. Technol.*, vol. 15, no. 2, pp. 803–815, Mar. 2020.
- [9] Y. Yoon and Z. W. Geem, "Parameter optimization of single-diode model of photovoltaic cell using memetic algorithm," *Int. J. Photoenergy*, vol. 2015, pp. 1–7, Nov. 2015.
- [10] H. Shin and Z. Geem, "Optimal design of a residential photovoltaic renewable system in South Korea," *Appl. Sci.*, vol. 9, no. 6, p. 1138, 1138.
- [11] Z. W. Geem and Y. Yoon, "Harmony search optimization of renewable energy charging with energy storage system," *Int. J. Electr. Power Energy Syst.*, vol. 86, pp. 120–126, Mar. 2017.
- [12] Z. G. Geem, "Size optimization for a hybrid photovoltaic-wind energy system," *Int. J. Electr. Power Energy Syst.*, vol. 42, pp. 448–451, Nov. 2012.
- [13] A. J. Gallego and E. F. Camacho, "Adaptative state-space model predictive control of a parabolic-trough field," *Control Eng. Pract.*, vol. 20, no. 9, pp. 904–911, Sep. 2012.
- [14] E. F. Camacho, F. R. Rubio, M. Berenguel, and L. Valenzuela, "A survey on control schemes for distributed solar collector fields. Part I: Modeling and basic control approaches," *Sol. Energy*, vol. 81, no. 10, pp. 1240–1251, Oct. 2007.
- [15] L. A. Barcia, R. P. Menéndez, J. Á. M. Esteban, M. A. J. Prieto, J. A. M. Ramos, F. J. De Cos Juez, and A. N. Reviriego, "Dynamic modeling of the solar field in parabolic trough solar power plants," *Energies* vol. 8, no. 12, pp. 13361–13377, 2015.
- [16] E. F. Camacho, F. R. Rubio, M. Berenguel, and L. Valenzuela, "A survey on control schemes for distributed solar collector fields—Part II: Advanced control approaches," *Sol. Energy*, vol. 81, no. 10, pp. 1252–1272, Oct. 2007.
- [17] T. A. Johansen, K. J. Hunt, and I. Petersen, "Gain-scheduled control of a solar power plant," *Control Eng. Pract.*, vol. 8, no. 9, pp. 1011–1022, Sep. 2000.
- [18] E. F. Camacho and M. Berenguel, "Application of generalized predictive control to a solar power plant," in *Proc. IEEE Int. Conf. Control Appl. CCA*, Aug. 1994, pp. 1657–1662.
- [19] R. N. Silva, L. M. Rato, and J. M. Lemos, "Time scaling internal state predictive control of a solar plant," *Control Eng. Pract.*, vol. 11, no. 12, pp. 1459–1467, Dec. 2003.
- [20] A. Alsharkawi and J. A. Rossiter, "Dual mode MPC for a concentrated solar thermal power plant," *IFAC-PapersOnLine*, vol. 49, no. 7, pp. 260–265, 2016.
- [21] E. F. Camacho, F. R. Rubio, and F. M. Hughes, "Self-tuning control of a solar power plant with a distributed collector field," *IEEE Control Syst. Mag.*, vol. 12, no. 2, pp. 72–78, Apr. 1992.
- [22] L. F. Dominguez, F. Klasing, and M. Mercangoz, "Modeling and control of a linear fresnel collector system," in *Proc. Eur. Control Conf. (ECC)*, Jun. 2014, pp. 1042–1048.
- [23] A. Arousseau, V. Vuillerme, and J.-J. Beziau, "Control systems for direct steam generation in linear concentrating solar power plants—A review," *Renew. Sustain. Energy Rev.*, vol. 56, pp. 611–630, Apr. 2016.
- [24] L. Valenzuela, E. Zarza, M. Berenguel, and E. F. Camacho, "Control concepts for direct steam generation in parabolic troughs," *Sol. Energy*, vol. 78, no. 2, pp. 301–311, Feb. 2005.
- [25] M. Eck and T. Hirsch, "Dynamics and control of parabolic trough collector loops with direct steam generation," *Sol. Energy*, vol. 81, no. 2, pp. 268–279, Feb. 2007.
- [26] G. Pellegrinetti and J. Bentsman, "Nonlinear control oriented boiler modeling—A benchmark problem for controller design," *IEEE Trans. Control Syst. Technol.*, vol. 4, no. 1, pp. 57–64, Jan. 1996.
- [27] T. D. Younkins and J. H. Chow, "Multivariable feedwater control design for a steam generator," *IEEE Control Syst. Mag.*, vol. 8, no. 2, pp. 77–80, Apr. 1988.
- [28] S. Kannaiyan, S. Bhartiya, and M. Bhushan, "Dynamic modeling and simulation of a hybrid solar thermal power plant," *Ind. Eng. Chem. Res.*, vol. 58, no. 18, pp. 7531–7550, May 2019.
- [29] K. M. Powell and T. F. Edgar, "Modeling and control of a solar thermal power plant with thermal energy storage," *Chem. Eng. Sci.*, vol. 71, pp. 138–145, Mar. 2012.
- [30] H. Liang, M. Fan, S. You, W. Zheng, H. Zhang, T. Ye, and X. Zheng, "A Monte Carlo method and finite volume method coupled optical simulation method for parabolic trough solar collectors," *Appl. Energy*, vol. 201, pp. 60–68, Sep. 2017.
- [31] W. Zheng, L. Yang, H. Zhang, S. You, and C. Zhu, "Numerical and experimental investigation on a new type of compound parabolic concentrator solar collector," *Energy Convers. Manage.*, vol. 129, pp. 11–22, Dec. 2016.
- [32] S. Kannaiyan, M. Bhushan, and S. Bhartiya, "Nonlinear state and parameter estimation for parabolic trough collector," in *Proc. ACODS Conf. IFAC*, 2018, pp. 453–459.
- [33] V. Chatoorgoon, "SPORTS—A simple non-linear thermohydraulic stability code," *Nucl. Eng. Des.*, vol. 93, no. 1, pp. 51–67, May 1986.
- [34] S. D. Odeh, G. L. Morrison, and M. Behnia, "Modelling of parabolic trough direct steam generation solar collectors," *Sol. Energy*, vol. 62, no. 6, pp. 395–406, Jun. 1998.
- [35] R. Haber, J. A. Rossiter, and K. Zabet, "An alternative for PID control: Predictive functional Control—A tutorial," in *Proc. Amer. Control Conf. (ACC)*, Jul. 2016, pp. 6935–6940.
- [36] S. W. Kieffer, "Sound speed in liquid-gas mixtures: Water-air and water-steam," *J. Geophys. Res.*, vol. 82, no. 20, pp. 2895–2904, Jul. 1977.
- [37] D. R. H. Beattie and P. B. Whalley, "A simple two-phase frictional pressure drop calculation method," *Int. J. Multiphase Flow*, vol. 8, no. 1, pp. 83–87, Feb. 1982.
- [38] M. Holmgren. *X Steam—Thermodynamic Properties of Water and Steam*. Accessed: Sep. 2018. [Online]. Available: <https://www.mathworks.com/matlabcentral/fileexchange/9817-x-steam-thermodynamic-properties-of-water-and-steam>
- [39] A. Chenu, K. Mikityuk, and R. Chawla, "Pressure drop modeling and comparisons with experiments for single- and two-phase sodium flow," *Nucl. Eng. Des.*, vol. 241, no. 9, pp. 3898–3909, Sep. 2011.

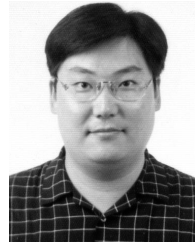
- [40] Q. Yan, E. Hu, Y. Yang, and R. Zhai, "Dynamic modeling and simulation of a solar direct steam-generating system," *Int. J. Energy Res.*, vol. 34, no. 15, pp. 1341–1355, Dec. 2010.
- [41] A. Aurousseau, V. Vuillerme, and J.-J. Beziau, "Modeling of linear concentrating solar power using direct steam generation with parabolic-trough," in *Proc. 11th Int. Modelica Conf.*, Versailles, France, Sep. 2015, pp. 595–603.



SURENDER KANNAIYAN was born in India in 1982. He received the B.E. degree in electronics and communication engineering from Bharathidasan University, in 2004, and the M.Tech. degree from the National Institute of Technology, Trichy, in 2006. He is currently an Assistant Professor with the Electronics and Communication Department, Visvesvaraya National Institute of Technology, Nagpur, India. His research interest includes dynamic modeling of renewable energy resources, control, and instrumentation.



NEERAJ DHANRAJ BOKDE received the M.E. degree in embedded systems from the EEE Department, BITS Pilani, Pilani Campus, India, and the Ph.D. degree from the Electronics and Communication Department, Visvesvaraya National Institute of Technology, Nagpur, India. He is currently a Postdoctoral Researcher with the Department of Engineering, Renewable Energy and Thermodynamics, Aarhus University, Denmark. His research interests include time series analysis, data mining, and prediction methodologies. He is serving as a Guest Editor in the *Energies* journal.



ZONG WOO GEEM (Member, IEEE) received the B.Eng. degree from Chung-Ang University, the Ph.D. degree from Korea University, and the M.Sc. degree from Johns Hopkins University. He researched at Virginia Tech, the University of Maryland at College Park, and Johns Hopkins University. He is currently an Associate Professor with the Department of Energy IT, Gachon University, South Korea. He invented a music-inspired optimization algorithm, Harmony Search, which has been applied to various scientific and engineering problems. His research interest includes phenomenon-mimicking algorithms and their applications to energy, environment, and water fields. He has served various journals as an editor (Associate Editor for *Engineering Optimization*; Guest Editor for *Swarm & Evolutionary Computation*, the *International Journal of Bio-Inspired Computation*, the *Journal of Applied Mathematics*, *Applied Sciences*, and *Sustainability*).

...